Research Square

Preprints are preliminary reports that have not undergone peer review.
They should not be considered conclusive, used to inform clinical practice,
or referenced by the media as validated information.

Phosphorylation of dynamin-related protein 1 at Ser616 promotes autophagy to suppress Mycobacterium tuberculosis survival via the ROS/HIF-1α axis in macrophages

Qianna Li
Southern Medical University
Qi Wang
Southern Medical University
Binchi Mo
Southern Medical University
Bo Zhu
Southern Medical University
Lingming Lin
Southern Medical University
Hongxuan Li
Southern Medical University
Jintang He
Southern Medical University
Shuo Chen
Southern Medical University
Zhenyu Han
Southern Medical University
Minna Xu
Southern Medical University
Qian Wen
Southern Medical University
Liang Zhou
Southern Medical University
Chaoying Zhou
Southern Medical University
Li Ma
Southern Medical University

Xinying Zhou

zxyforever@smu.edu.cn

Southern Medical University

Research Article

Keywords: Dynamin-related protein 1 (Drp1), Mycobacterium tuberculosis (Mtb), macrophages, autophagy, reactive oxygen species (ROS), hypoxia-inducible factor-1alpha (HIF-1α)

Posted Date: August 10th, 2026

DOI: https://doi.org/10.21203/rs.3.rs-10550606/v1

License: This work is licensed under a Creative Commons Attribution 4.0 International License. Read Full License

Additional Declarations: No competing interests reported.

Phosphorylation of dynamin-related protein 1 at Ser616 promotes autophagy to suppress *Mycobacterium tuberculosis* survival via the ROS/HIF-1α axis in macrophages

Qianna Li[a,b,c #], Qi Wang[a,b,c #], Binchi Mo[a,b,c #], Bo Zhu[a,b,c], Lingming Lin[a,b,c], Hongxuan Li[a,b,c], Jintang He[a,b,c], Shuo Chen[a,b,c], Zhenyu Han[a,b,c], Minna Xu[a,b,c], Qian Wen[a,b,c], Liang Zhou[a,b,c], Chaoying Zhou[a,b,c], Li Ma[a,b,c]*, Xinying Zhou[a,b,c]*

[a]Institute of Molecular Immunology, School of Laboratory Medicine and Biotechnology, Southern Medical University, Guangzhou 510515, China.

[b]Key Laboratory of Infectious Diseases Research in South China, Ministry of Education, Southern Medical University, Guangzhou 510515, China.

[C]State Key Laboratory of Multi-organ Injury Prevention and Treatment, Southern Medical University, Guangzhou 510515, China

Short Title: Drp1 phosphorylation promotes autophagy against Mtb

# These authors contributed equally to this work.

*Corresponding author:

Dr. Xinying Zhou

Xinying Zhou, PhD, Institute of Molecular Immunology, School of Laboratory Medicine and Biotechnology, Southern Medical University, Guangzhou 510515, China. Phone: +86-20-61648553, Fax: +86-20- 61648555. E-mail: zxyforever@smu.edu.cn

Dr. Li Ma

Li Ma, PhD, Institute of Molecular Immunology, School of Laboratory Medicine and Biotechnology, Southern Medical University, Guangzhou 510515, China. Phone: +86-20-61648322, Fax: +86-20-61648322. E-mail: mali_61648322@smu.edu.cn

Number of Figures: 8

Keywords: Dynamin-related protein 1 **(**Drp1), *Mycobacterium tuberculosis* (Mtb), macrophages, autophagy, reactive oxygen species (ROS), hypoxia-inducible factor-1alpha (HIF-1α).

Abstract

Tuberculosis (TB), caused by *Mycobacterium tuberculosis* (Mtb), remains a leading cause of global mortality from a single infectious agent. The mitochondrial fission protein dynamin-related protein 1 (Drp1) is known to modulate host immunity, but its role in anti-mycobacterial defense is unclear. Here, we found that Mtb infection triggers Drp1 phosphorylation at Ser616 in macrophages and TB patient tissues. Genetic or pharmacological inhibition of Drp1 enhanced intracellular Mtb survival, whereas Drp1 overexpression restricted bacterial loads. Myeloid-specific Drp1 knockout mice exhibited exacerbated pulmonary infection and inflammation. Mechanistically, Drp1 promoted xenophagic clearance of Mtb, as evidenced by increased LC3-II lipidation, p62 recruitment to Mtb, lysosomal-associated membrane protein 1 (LAMP1) colocalization with bacteria, and chloroquine-sensitive autophagic flux. Mechanistically, Drp1 promoted xenophagic clearance of Mtb, as evidenced by increased LC3-II lipidation, p62 recruitment to Mtb, LAMP1 colocalization with bacteria, and chloroquine-sensitive autophagic flux. These effects were independent of AMP-activated protein kinase (AMPK)/mechanistic target of rapamycin (mTOR) and Parkin pathways but required ROS production and hypoxia-inducible factor-1α (HIF-1α) stabilization, as ROS scavenging abolished, while HIF-1α activation restored Drp1-mediated autophagy and bacterial control. Carbonyl cyanide m-chlorophenyl hydrazine (CCCP) treatment rescued autophagic flux and bacterial killing in Drp1-silenced cells. Importantly, a phosphorylation-deficient S616A mutant failed to promote ROS

production, HIF-1α stabilization, autophagic flux, lysosomal delivery, and Mtb clearance, identifying Ser616 phosphorylation as the critical switch. Together, these findings identify phosphorylated Drp1 (S616) as a key upstream regulatory node in macrophage anti-tuberculosis immunity and provide a mechanistic basis for targeting Drp1 S616 phosphorylation as a potential host-directed therapeutic strategy against TB.

Abbreviations: Drp1: Dynamin-related protein 1; Mtb: Mycobacterium tuberculosis; ROS: reactive oxygen species; HIF-1α: hypoxia-inducible factor-1alpha; TB: tuberculosis LC3-II: Microtubule-associated protein 1 light chain 3-II; MA: 3-Methyladenine; AMPK: AMP-activated protein kinase; mTOR: Mechanistic target of rapamycin; Parkin: encoded by the PARK2 gene; NAC: N-Acetyl-Cysteine; CCCP: Carbonyl cyanide m-chlorophenyl hydrazo; Mfn1: Mitofusin 1; Mfn2: Mitofusin 2; OPA1: Optic atrophy 1; Fis1: Fission 1 protein; Mff: Mitochondrial fission factor; MiD49: encoded by gene Mief2; MiD51: encoded by gene Mief1; p-Drp1: phosphorylated Drp1; Drp1 cKO: $Dnm1l^{Lyz2\text{-}cre}$; Lyz2-iCre: the lysozyme M promoter-driven codon-improved Cre recombinase; $Dnm1l^{fl/fl}$: the Dnm1l conditional knockout; Dnm1lLyz2-cre: macrophage-specific Dnm1l knockout mice; BMDMs: bone marrow-derived macrophages; DMEM: Dulbecco's Modified Eagle Medium; FBS: fetal bovine serum; GM-CSF: granulocyte-macrophage colony-stimulating factor; RAW264.7: the murine macrophage cell line; ATCC: the American Type Culture Collection; H37Rv: The Mtb reference strain; PBS: phosphate-buffered saline; OD600: the optical density

71 at 600 nm; i.p.: intraperitoneal; CFU: colony-forming units; MOI: at the specified
72 multiplicity of infection; Mdivi-1: Mitochondrial division inhibitor 1; L-NAME: N ω -
73 Nitro-L-arginine methyl ester; DMSO: dimethylsulfoxide; siRNA: Short Interfering
74 RNA; BFP: blue fluorescent protein; BSA: bovine serum albumin; ELISA: Enzyme-
75 linked immunosorbent assay; DCFH-DA: 2′,7′-dichlorodihydrofluorescein
76 diacetate; NO: Nitric oxide; NED: N-1-naphthylethylenediamine dihydrochloride;
77 BCA: bicinchoninic acid; PVDF: polyvinylidene difluoride; PBST: PBS containing 0.1%
78 Tween-20; HRP: horseradish peroxidase; ECL: chemiluminescence; DAPI: 4, 6-
79 diamidino-2-phenylindole; IOD: integrated optical density; SD: standard deviation;
80 ANOVA: one-way analysis of variance; GFP: green fluorescent protein; mtDNA:
81 mitochondrial DNA; mtRNA: mitochondrial RNA; mito-DAMPs: mitochondrial
82 damage-associated molecular patterns; RLR: RIG-I-like receptor; Atg: autophagy-
83 related; VMP1: vacuole membrane protein 1; PE: phosphatidylethanolamine; Thbs-1:
84 Thrombospondin-1

85

Introduction

Tuberculosis (TB), caused by *Mycobacterium tuberculosis* (Mtb), remains the leading cause of death from a single infectious agent globally, representing a major and ongoing threat to public health[1]. The management of TB is hampered by the prolonged duration of chemotherapy, substantial drug side effects, and limited treatment options for drug-resistant strains. A fundamental challenge in improving TB control is an incomplete understanding of the complex interplay between Mtb and host immunity. Macrophages, central to the innate immune response, serve as a critical double-edged sword: they are the primary cellular niche for Mtb survival and replication, yet also possess the capacity to eliminate the pathogen[2]. Consequently, elucidating the innate defense mechanisms of macrophages against Mtb, alongside the bacterial strategies that subvert these defenses to permit intracellular persistence, is essential for identifying novel therapeutic targets and advancing more effective strategies against TB.

Multiple studies have demonstrated that Mtb infection disrupts the mitochondrial network within macrophages, inducing metabolic alterations and influencing innate immune signaling[3]. Mitochondrial homeostasis is maintained through a continuous cycle of fusion and fission, a process meticulously regulated by specific proteins and critical for modulating host immune responses[4]. Mitochondrial fusion is mediated by the outer membrane proteins Mitofusin 1 (Mfn1) and Mitofusin 2 (Mfn2), and the inner membrane protein Optic atrophy 1 (OPA1). Conversely, fission is primarily executed

by Dynamin-related protein 1 (Drp1, encoded by *Dnm1l*). Upon activation by phosphorylation, cytosolic Drp1 is recruited to outer mitochondrial membrane receptors, including Fission 1 protein (Fis1), Mitochondrial fission factor (Mff), MiD49 (encoded by *Mief2*), and MiD51 (encoded by *Mief1*), to initiate membrane constriction and division[4]. Dysregulation of this fusion-fission balance leads to mitochondrial damage, perturbing critical cellular processes such as metabolism, apoptosis, and autophagy, thereby shaping the host immune response and the progression of infectious diseases[5]. While roles for the fusion protein Mfn2 in regulating the innate immune response to Mtb have been described[6, 7], the effects and precise mechanisms of the key fission protein Drp1 in host defense against Mtb infection remain to be fully characterized.

Drp1 plays a vital role in regulating immune responses across various cell types, including macrophages, NK cells, and T cells[8-10]. Notably, Drp1 is implicated in modulating autophagy, a cellular degradation process critical for the clearance of intracellular pathogens[11-13]. Autophagy is crucial for anti tuberculosis immunity by directly eliminating the pathogen, regulating immune responses, and suppressing inflammatory damage to combat Mtb infection. However, it remains unclear whether Drp1 mediates its anti mycobacterial function specifically through the regulation of xenophagy—the selective autophagic clearance of intracellular pathogens—and if so, through which downstream signaling pathways. Furthermore, although Drp1 phosphorylation is known to regulate its activity, the functional relevance of specific

phosphorylation sites in the context of Mtb infection has not been directly addressed.

Our investigation reveals that Mtb infection triggers Drp1 phosphorylation at Ser616 in macrophages, a response observed both in vitro and in clinical samples from TB patients. Through combinatorial in vitro and in vivo genetic manipulation, we demonstrate that this phosphorylation event serves as a critical molecular switch that activates a ROS–HIF-1α signaling cascade to promote xenophagic clearance of intracellular Mtb. Collectively, this study establish Drp1 as a novel innate immune effector against Mtb and provide mechanistic insights that may inform the development of host-directed therapeutic strategies for tuberculosis.

Materials and Methods

Ethics statement

This study was conducted in accordance with recommendations for human research by the International Committee of Medical Journal Editors and for animal research by the National Institutes of Health Guide for the Care and Use of Laboratory Animals. The protocol was reviewed and approved by the Ethics Committee and the Biosafety Management Committee of Southern Medical University. All work with highly pathogenic microorganisms was performed under an approved laboratory management commitment letter from Southern Medical University.

Clinical characteristics of study participants.

All enrolled participants, including tuberculosis (TB) patients and control subjects, were diagnosed and recruited at the Guangzhou Chest Hospital (Guangzhou, Guangdong, China). A total of 18 individuals were included in this study: 6 patients with pulmonary tuberculosis (PTB), 6 patients with lymph node tuberculosis (LNTB), and 6 control subjects with pneumonia. TB patients were diagnosed based on positive Mtb culture, acid-fast bacilli (AFB) staining, Mtb PCR, and/or compatible clinical symptoms. Control subjects were pneumonia patients with non-infectious pulmonary diseases and were confirmed negative for Mtb infection by pathological examination and/or PCR. Detailed demographic and clinical information, including age, sex, diagnosis, sample type, AFB staining, Mtb culture results, and Mtb PCR results, are summarized in Supplementary Table 1. Abbreviations used in the table are defined in

158 the footnotes.

159 **Mice**

160 C57BL/6J mice were obtained from the Laboratory Animal Center of Southern Medical
161 University (Guangzhou, China). All mice were housed in specific pathogen–free
162 conditions within the same center. Both the lysozyme M promoter-driven codon-
163 improved *Cre* recombinase (*Lyz2-iCre*, Strain NO. T003822) mice and the *Dnm1l*
164 conditional knockout ($Dnm1l^{fl/fl}$, Strain NO. T052330) mice were procured from the
165 same source, GemPharmatech Co., Ltd. (Nanjing, China). $Dnm1l^{fl/fl}$ mice and *Lyz2-iCre*
166 mice were both maintained on a congenic C57BL/6JGpt background. To generate
167 macrophage-specific *Dnm1l* knockout mice ($Dnm1l^{Lyz2\text{-}cre}$), $Dnm1l^{fl/fl}$ mice were
168 crossed with Lyz2-iCre mice. Littermate $Dnm1l^{fl/fl}$ mice lacking the Cre transgene were
169 used as controls in all experiments.

170 ***In vitro* differentiation of mouse macrophages**

171 Bone marrow-derived macrophages (BMDMs) were generated from the femurs and
172 tibiae of 4- to 6-week-old female C57BL/6J mice (obtained from the Southern Medical
173 University Animal Experimental Center). Cells were differentiated into macrophages
174 in Dulbecco's Modified Eagle Medium (DMEM) supplemented with 10% fetal bovine
175 serum (FBS), 100 ng/mL granulocyte-macrophage colony-stimulating factor (GM-
176 CSF), and 1% Penicillin-Streptomycin. The medium was replaced with fresh
177 differentiation medium on days 3 and 5. After 7 days of culture, adherent BMDMs were
178 detached using trypsin-EDTA (Solarbio, Beijing, China), resuspended in complete

DMEM (containing 10% FBS), and seeded into 12-well or 6-well plates for subsequent experiments. The murine macrophage cell line RAW264.7 (ATCC® TIB-71™) was acquired from the American Type Culture Collection (ATCC).

Mtb culture and infection

The Mtb reference strain H37Rv (American Type Culture Collection 25618) and BCG (SINOPHARM, Beijing, BJ, China) were cultured in Middlebrook 7H9 broth (Becton Dickinson, USA) supplemented with 0.2% glycerol (GHTECH, China), 10% OADC enrichment, and 0.05% Tween 80. Cultures were incubated at 37°C with 5% CO_2. The OADC supplement consisted of 0.06% (v/v) oleic acid, 5% bovine serum albumin fraction V, 2% dextrose, 0.003% catalase, and 0.85% NaCl (all from Sigma-Aldrich, USA, unless otherwise noted). For infection, mid-log phase bacterial cultures were gently vortexed with 3-mm glass beads to disperse clumps. The bacterial suspension was then centrifuged, and the pellet was resuspended in sterile phosphate-buffered saline (PBS) or cell culture medium. After brief low-speed centrifugation to remove remaining aggregates, the optical density at 600 nm (OD_{600}) of the single-cell suspension was measured using a microplate reader (Thermo Fisher Scientific, USA). The bacterial concentration was calculated from a standard OD_{600}-to-CFU curve. Cells were infected at the specified multiplicity of infection (MOI) by adding the prepared bacterial inoculum.

***In vivo* mouse infection model**

Drp1 conditional knockout mice and their littermate controls (6-8 weeks old, 18-25 g

body weight) were housed under specific pathogen-free conditions with a 12-hour light/dark cycle and provided food and water ad libitum. All mice were infected via the nose-only inhalation route using an aerosol drug delivery system (model AER-S-NSST6; Shanghai TOW Intelligent Technology Co., Ltd., Shanghai, China). For infection, the bacterial suspension (1×10^6 CFU/mL) was loaded into the AER aerosol generator. Mice were individually restrained in nose-only holders (model NOE-Holder-M; Shanghai TOW) and exposed to the aerosolized bacteria for 10 minutes. The exposure tower was connected to an exhaust gas treatment assembly to prevent environmental contamination with Mtb. The entire procedure was performed inside a Class II biological safety cabinet. Beginning on the day of infection, mice received daily intraperitoneal (i.p.) injections of either Mdivi-1 (20 mg/kg) or an equivalent volume of PBS vehicle control. At one and three weeks post-infection, mice were euthanized. Lungs and spleens were aseptically harvested and homogenized in sterile PBS. Serial dilutions of the tissue homogenates were plated onto Middlebrook 7H10 agar plates supplemented with 10% OADC. Plates were incubated at 37℃ in a 5% CO_2 atmosphere for 3-4 weeks, after which visible bacterial colonies were counted to determine the organ CFU burden.

Treatment of reagents in macrophages

BMDMSs and RAW264.7 cells were pretreated with inhibitor of Drp1 for Mitochondrial division inhibitor 1 (Mdivi-1) (200 nM) (Selleck, USA), inhibitor of Autophagy for 3-MA (10 mM) (Selleck, USA), inhibitor of Oxidative phosphorylation

for CCCP (10 μM) (Selleck, USA), inhibitor of HIF-α for Roxadustat (50 μM) (Selleck, USA), inhibitor of ROS for NAC (5 mM) (Selleck, USA), inhibitor of NO for Nω-Nitro-L-arginine methyl ester (L-NAME) (50 μM) (Selleck, USA) and dimethylsulfoxide (DMSO) as solvent control for corresponding processing time before H37Rv infection. Pre-processing time and other details of the reagents are shown in **Supplementary Table 2**.

Colony-forming unit assays

H37Rv was collected through low-speed centrifugation (3000 rpm.) from 7H9 (broth, Becton Dickinson, New Jersey, USA) liquid nutrient medium. H37Rv was suspended with DMEM (10% FBS) and transferred into grinder to generate a single bacterial suspension. The density of bacteria was measured by spectrophotometer in OD_{600}. BMDMs or RAW264.7 cells infected with Mtb at MOI of 5 for 1 hour were seeded in 12-well culture plate. Extracellular bacteria were removed with PBS washing three times. Cells were continued to culture with fresh DMEM (10% FBS) media or media with different drugs or inhibitors. Then, the cells were lysed at the indicated time-points with 0.01% Triton X-100 (Solarbio, Beijing, China). Lysates were transfer into 7H10 agar plates containing 10% OADC (Becton Dickinson, New Jersey, USA) in serial dilution. The bacteria colonies were counted after the 7H10 agar plate incubated upside down in 5% CO_2 incubator at 37℃ for 3-4 weeks.

Transfection of cells with siRNAs

BMDM and RAW264.7 cells were seeded in 12-well cell culture in density of 5×10^5

for 24 hrs in incubator. Relevant Short Interfering RNA (siRNA) was synthetized by RiboBio (Guangzhou, China) according to NCBI gene database. Si RNA was dissolved in opti-MEM (Gibco, Life Technologies, NY, USA) for 100 nM and mixed with Lipofectamine 2000 (Thermo Fisher Scientific, Carlsbad, CA, USA) According to manufacturer.The solution was mixed gently and thoroughly. After incubation at room temperature for 20 min, transfection buffer was added dropwise into the differentiated macrophages and inoculated for 4 to 6 hrs.

Lentiviral-Mediated overexpression

Lentiviral particles were generated using the X-tremeGENE HP DNA transfection reagent (Roche, Switzerland) according to the manufacturer's protocol.

Drp1 overexpression and S616A mutant generation: RAW264.7 macrophages were transduced with lentiviral particles encoding either wild-type Drp1 (WT) or a phosphorylation-deficient mutant (S616A) using the pHAGE-mDNM1L-Flag_IRES_PuroR backbone (OBiO Technology, China). The S616A mutant was generated by site-directed mutagenesis. Lentiviral packaging was performed in HEK293T cells using X-tremeGENE HP (Roche) with packaging plasmids pMD2.G and psPAX2. Cells were seeded at 5×10^5 cells per well in 6-well plates and transduced at an MOI of 20 for 72 hours, followed by puromycin selection (2 μg/mL, 7 days). Stable protein expression was verified by Western blotting with anti-Flag and anti-DRP1 antibodies.

Parkin Overexpression: For Parkin overexpression, the pLenti-CMV-EBFP-

3FLAG vector encoding human PARK2 (Parkin) was used. RAW264.7 cells were seeded in 6-well plates at a density of 5×10^5 cells per well. Cells were transduced with lentiviral particles at a MOI of 20 for 72 hrs at 37°C. Transduced cells positive for the blue fluorescent protein (BFP) marker were isolated using flow cytometry on a MoFlo XDP sorter (Beckman Coulter, USA).

Flow Cytometric Analysis of Surface Markers

Cell suspensions were prepared for flow cytometric analysis as described below. All staining steps were performed in the dark. Data were acquired on a BD LSRFortessa X-20 cytometer and analyzed using FlowJo software. Surface Marker Staining: Cells were harvested, washed twice with PBS containing 1% bovine serum albumin (BSA; staining buffer), and resuspended in 100 µL of staining buffer. Cells were incubated with fluorescently conjugated monoclonal antibodies (mAbs) or isotype-matched controls for 30 minutes at 4°C. The following anti-mouse surface antibodies were used: CD80 (Clone 16-10A1, eFluor 450; Invitrogen), CD86 (Clone GL1, APC; eBioscience), CD200R (Clone OX110, PE; eBioscience), and F4/80 (Clone BM8.1, FITC; TONBO). After incubation, cells were washed twice and resuspended in staining buffer. Intracellular staining for CD206: following surface staining, cells were fixed and permeabilized using the Intracellular Fixation & Permeabilization Buffer Set (Thermo Fisher Scientific) according to the manufacturer's instructions. Cells were then stained intracellularly with an anti-CD206 antibody (Clone 34-1-2S, PerCP-eFluor 710; Invitrogen) for 1 hour at 4°C, washed, and resuspended in PBS staining buffer.

Intracellular Cytokine Staining: for cytokine detection, harvested cells were restimulated in vitro with a Cell Stimulation Cocktail (containing PMA/ionomycin and protein transport inhibitors; Thermo Fisher Scientific) for 6 hrs at 37°C under 5% CO_2. Cells were first stained for surface markers using CD4 (Clone RM4-5, PerCP-Cy5.5; TONBO) and CD8a (Clone 53-6.7, Pacific Blue; BioLegend) antibodies. Cells were then fixed, permeabilized (using the same buffer set as above), and stained intracellularly with antibodies against IFN-γ (Clone XMG1.2, FITC; BioLegend), IL-4 (Clone 11B11, PE; BioLegend), and IL-17A (Clone eBio17B7, APC; eBioscience).

Enzyme-linked immunosorbent assay (ELISA) assay

Cell culture supernatants and mouse lung tissue homogenates were collected in 1.5 mL microcentrifuge tubes. To remove residual Mycobacterium tuberculosis H37Rv, samples were filtered through a 0.22 μm membrane filter. The concentrations of secreted IL-6, IL-1β, TNF-α, and IL-10 were quantified using commercial ELISA kits (MultiSciences, Guagnzhou, China). All assays were performed strictly according to the manufacturers' protocols. Absorbance was measured at 450 nm and 630 nm using a TECAN SPARK microplate reader (Tecan, Austria). Sample cytokine concentrations were determined by interpolating the 450 nm (reference-corrected) optical density values against a standard curve generated for each assay.

Measurement of Mitochondrial Membrane Potential (ΔΨm)

The mitochondrial membrane potential (ΔΨm) was assessed using the JC-1 probe (C2006, Beyotime, China). Briefly, RAW 264.7 macrophages were seeded in 6-well

plates and subjected to different treatments: cells were either infected with M. bovis BCG at a multiplicity of infection (MOI) of 5 for 6 h, or treated with 10 μM carbonyl cyanide m-chlorophenylhydrazone (CCCP) for 30 min at 37°C to induce complete mitochondrial depolarization as a positive control. After the respective treatments, cells were harvested, washed twice with PBS, and incubated with JC-1 staining working solution (5 μg/mL) at 37°C for 20 min in the dark. Subsequently, cells were washed twice with JC-1 staining buffer to remove excess dye. For immunofluorescence analysis, the fluorescence shift from red (aggregates, indicating high ΔΨm) to green (monomers, indicating low ΔΨm) was immediately visualized using a Nikon AX confocal microscope (Nikon Corporation, Tokyo, Japan) with excitation/emission at 488/530 nm (green) and 561/590 nm (red). The results are expressed as the ratio of red to green fluorescence intensity, which reflects the relative ΔΨm. A decrease in this ratio indicates mitochondrial depolarization. For flow cytometric analysis, to precisely quantify the average fluorescence intensity of the entire cell population, stained cells were resuspended in PBS and analyzed on a BD LSRFortessa X-20 cytometer. JC-1 green fluorescence (FL-1 channel) and red fluorescence (FL-2 channel) were recorded for at least 10,000 events per sample. Data were analyzed using FlowJo software (BD Biosciences). The ΔΨm was expressed as the ratio of mean fluorescence intensity (MFI) of red to green (FL-2/FL-1), providing a more accurate and statistically robust quantitative assessment of mitochondrial depolarization across the whole cell population. The CCCP-treated group served as a positive control to validate the assay's

responsiveness, while the uninfected group served as the negative control to establish the baseline ΔΨm level.

Detection of Mitochondrial Reactive Oxygen Species (mtROS)

Mitochondrial superoxide levels were measured using a MitoSOX™ Red mitochondrial superoxide detection kit (M36008, Thermo Fisher Scientific, USA). Cells were seeded into 12-well plates at a density of 1×10^5 cells per well and cultured in a humidified incubator at 37 °C with 5% CO_2 for 24 hrs to allow adherence. Following preparation of a single-cell suspension of M. bovis BCG, cells were infected at a MOI of 5 for 6 hrs. The culture medium was then aspirated, and cells were washed once with phosphate-buffered saline (PBS). As a positive control, mSoxUp (1000×) provided in the kit was added to the cell culture medium at a dilution of 1:1000, and cells were treated for 4 h. MitoSOX™ Red staining working solution was prepared by diluting MitoSOX™ Red (5 mM) in PBS at a ratio of 1 μl per 1 ml PBS, followed by thorough mixing. One milliliter of the MitoSOX™ Red working solution was added to each well, and cells were incubated at 37 °C in the dark for 30 min. Following incubation, the supernatant was aspirated, and cells were washed twice with 1 ml of PBS. Cells were then resuspended in 1% fetal bovine serum (FBS) in PBS, and the cell suspension was collected. Fluorescence intensity was detected using a BD LSRFortessa X-20 flow cytometer, and data were analyzed with FlowJo software.

Assessment of Mitochondrial DNA (mtDNA) Damage/ReleaseReactive oxygen

To evaluate mtDNA damage, we quantified the copy number of mtDNA relative to

nuclear DNA and/or the levels of oxidative DNA adduct 8-hydroxy-2'-deoxyguanosine (8-OHdG). Total DNA was extracted from macrophages 24 hrs post-infection using a DNA extraction kit (D3396-02, OMEGA, USA). mtDNA was quantified by qPCR using primers specific for the mitochondrial D-loop region, a specific region of mtDNA that is not inserted into nuclear DNA (non-NUMT). Nuclear DNA encoding telomerase reverse transcriptase (Tert), and β2 microglobulin (B2m) was used for normalization. The fold change in cytosolic mtDNA was calculated using the $2^{-\Delta\Delta Ct}$ method. The sequences for all gene-specific primers are listed in **Supplementary Table 3**.

Measurement of intracellular ROS levels

Intracellular ROS levels were measured using the fluorescent probe 2′,7′-dichlorodihydrofluorescein diacetate (DCFH-DA; Beyotime, S0033M, China). BMDMs or RAW264.7 macrophages were seeded in 6-well plates at a density of 5×10^5 cells per well. Twenty-four hours after seeding, cells were infected with Mtb H37Rv at a multiplicity of infection (MOI) of 2. At 6 hrs post-infection, cells were washed three times with warm DMEM and incubated with 10 μM DCFH-DA in serum-free medium for 30 min at 37 °C in the dark. After incubation, cells were washed with PBS, detached, and resuspended in PBS containing 1% FBS. Cellular fluorescence, reflecting ROS levels, was immediately analyzed using a BD LSRFortessa X-20 flow cytometer (BD Biosciences, USA). Data were processed and analyzed using FlowJo software (BD Life Sciences, USA).

Nitric oxide (NO) measurement

Nitric oxide production was assessed by measuring the accumulation of its stable oxidative metabolite, nitrite, in culture supernatants using the Griess Reagent System (Promega, USA), according to the manufacturer's instructions. A standard curve was prepared using sodium nitrite solution. For the assay, 50 µL of cell culture supernatant was transferred to a 96-well plate. An equal volume (50 µL) of sulfanilamide solution was added to each well, and the plate was incubated at room temperature for 5-10 min, protected from light. Subsequently, 50 µL of N-1-naphthylethylenediamine dihydrochloride (NED) solution was added to each well, followed by a second incubation under the same conditions. The absorbance was measured within 30 min using a Varioskan Flash microplate reader (Thermo Fisher Scientific, USA). The nitrite concentration in each sample was determined by subtracting the absorbance at 630 nm from the absorbance at 450 nm and interpolating the value against the standard curve.

Mitochondrial fluorescence microscopy

For mitochondrial imaging, BMDMs or RAW264.7 cells were seeded onto poly-L-lysine-coated glass coverslips (Thermo Fisher Scientific, USA). Following the appropriate experimental treatments, live cells were stained with MitoTracker Deep Red FM (Thermo Fisher Scientific, USA) in pre-warmed complete DMEM (10% FBS) according to the manufacturer’s recommended concentration and duration. Cells were subsequently fixed with 4% paraformaldehyde for 15 min at room temperature. For experiments requiring immunostaining, fixed cells were permeabilized with 0.2% Triton X-100 in PBS for 10 min. Confocal microscopy was performed using a Zeiss

LSM 880 system (Zeiss, Germany) equipped with a 63× oil immersion objective. Z-stack images were acquired to capture full cellular volume. For quantification, at least 20 cells per condition were imaged across five random fields of view. Mitochondrial morphology and fluorescence intensity were analyzed using FIJI/ImageJ software (National Institutes of Health, USA).

RNA Extraction and qRT-PCR analysis

Total RNA of macrophages was extracted by TRIzol Reagent or Total RNA Kit I (200) (OMEGA, Norcross, GA, USA) according to manufacturer. mRNA reverse into cDNA through Reverse transcription system (Novogene, Beijing, China). The expression mRNA level of the related gene was detected by a SYBR® Premix Ex TaqTM II (Tli RNaseH Plus) (TaKaRa, Beijing, China) on a LightCycler 480 thermocycler (Roche, Basel, Switzerland). The three-step qPCR condition involves an initial step at 95℃ for 120 s, followed by 35 cycles of amplification and quantification (95℃ for 15 s, 65℃ for 15 s, 68℃ for 20 s). Relative gene expression levels were calculated using the $2^{-\Delta\Delta Ct}$ method, with β-actin serving as the internal reference control. The sequences for all gene-specific primers are listed in **Supplementary Table 3**.

Western Blot Analysis

Following specific treatments, cells were washed once with PBS and lysed on ice using RIPA buffer supplemented with protease and phosphatase inhibitors. Alternatively, a protein lysis buffer containing 41.6 mM SDS (Zhuosheng Biotech, China), 455 mM Tris-HCl (pH 6.8; Sangon Biotech, China), 30% (v/v) glycerol (Sigma-Aldrich, USA),

and 10 mM DTT (Sigma-Aldrich, USA) was used for some experiments. Protein concentrations were determined using a bicinchoninic Acid (BCA) assay. Equal amounts of protein (typically 20-40 μg) were denatured by heating at 100°C for 10 minutes in Laemmli sample buffer. Proteins were then separated by electrophoresis on SDS-polyacrylamide gels of appropriate concentrations (e.g., 8-15%). After separation, proteins were transferred onto polyvinylidene difluoride (PVDF) membranes (Merck KGaA, Germany). Membranes were blocked for 1 hour at room temperature in PBS containing 0.1% Tween-20 (PBST) and either 5% (w/v) bovine serum albumin (BSA; Sigma-Aldrich, USA) or 5% (w/v) non-fat dried milk. Membranes were incubated overnight at 4℃ with gentle agitation in primary antibodies diluted 1:1000 in PBST with 5% BSA. Following three 10-min washes with PBST, membranes were incubated for 1 hour at room temperature with appropriate horseradish peroxidase (HRP)-conjugated secondary antibodies (Cell Signaling Technology, USA) diluted 1:2000 in PBST with 5% BSA. Protein bands were visualized using an enhanced chemiluminescence (ECL) substrate (Thermo Fisher Scientific, USA) according to the manufacturer's instructions, and images were captured using a FluorChem imaging system (ProteinSimple, USA). A complete list of primary and secondary antibodies used is provided in **Supplementary Table 4**.

Autopahgy flux assay

The mCherry–eGFP–LC3 adenovirus was obtained from Hanbio (Shanghai, China). RAW264.7 cells were seeded into 6-well plates at a density of 5×10^5 cells per well

and allowed to adhere. Cells were then transduced with the adenovirus at a MOI of 20 and incubated at 37 °C for 72 hrs. For imaging, cells were prepared on glass coverslips. Following transduction, nuclei were stained with DAPI (Sangon Biotech, Shanghai, China) for 10 min at room temperature. Cells were subsequently washed with 0.05% Tween-20 in PBS to remove excess stain. Cells were imaged by using a Zeiss LSM 880 confocal microscope (Zeiss, Göttingen, Germany) equipped with an Airyscan detector. Images were acquired and processed using the ZEN software (Zeiss) and analyzed with FIJI (ImageJ) software.

Immunofluorescence and Colocalization

For immunofluorescence staining, Mtb was first labeled with Texas Red (Thermo Fisher Scientific, USA) at a concentration of 10 μg/ml in PBS. RAW264.7 macrophages seeded on sterile glass coverslips in 24-well plates were then infected with the Texas Red-labeled bacteria at a multiplicity of infection (MOI) of 2 for 12 h. After infection, cells were washed twice with PBS, fixed with 4% paraformaldehyde for 10 min, and permeabilized with 0.2% Triton X-100 in PBS for 10 min at room temperature. Cells were then blocked with PBS containing 0.05% Tween-20 and 10% bovine serum albumin (BSA) for 30 min.

To examine autophagic recognition and lysosomal delivery of intracellular MTB, cells were incubated overnight at 4°C with primary antibodies against LC3B (Abclonal # A19665, 1:200), LAMP1 (Santa Cruz # sc-20011, 1:100), or p62 (Santa Cruz # sc-48402, 1:250). After primary antibody incubation, cells were washed three times with

PBS containing 0.05% Tween-20 and then incubated with Alexa Fluor® 488-conjugated donkey anti-rabbit IgG (H+L) or Alexa Fluor™ Plus 647-conjugated goat anti-mouse IgG (H+L) secondary antibodies (Invitrogen, USA) at room temperature for 30 min in the dark. Nuclei were counterstained with 4′,6-diamidino-2-phenylindole (DAPI) (Sangon Biotech, Shanghai, China) for 10 min at room temperature after removing excess secondary antibodies with 0.05% Tween-PBS. Coverslips were mounted onto glass slides using ProLong Gold antifade mounting medium (Thermo Fisher Scientific). Texas Red fluorescence served as the direct signal for MTB, eliminating the need for anti-MTB antibody staining.

Confocal images were acquired using a Zeiss Axiovert LSM 880 confocal microscope (Zeiss, Göttingen, Germany) and analyzed with FIJI software. Colocalization between Mtb (Texas Red) and LC3, LAMP1, or p62 was quantified by calculating the percentage of Mtb bacteria positive for each respective marker over total intracellular Mtb, from at least 10 random fields per condition and a minimum of 100 Mtb-containing cells per group across three independent experiments. Manders' colocalization coefficients were also calculated using the Coloc 2 plugin in FIJI. All primary antibodies used in this study are listed in Supplementary Table 2.

Immunohistochemistry Assay

Archived human lymph node and lung tissues were fixed in 10% formalin, embedded in paraffin wax and deparaffinized in xylene. For immunohistochemical staining, parraffin sections (4 μm) were heated with 0.01 M citric acid of pH 6.0 for 3 min for

antigen retrieval. The slices were treated with 3% H_2O_2 for 10 min to react with endogenous peroxidase. Sections were incubated with p-Drp1 (1:500, Cell Signaling Technology, UK) Ab overnight and secondary biotinylated anti-mouse (1: 50) followed by DAB substrate (UniCureLab). The slices were counterstained by hematoxylin and dehydrated by gradient alcohol. For slices of lungs, because the cells are relatively scattered and few, immunohistochemical staining for p-Drp1 was quantified by positive cell rate analysis by using Image Pro Plus 6.0 software (Media Cybernetics, Inc., Rockville, MD, USA). We analyzed the number of positive cells with the same brown-yellow cell nucleus and the total number of cells in each photo, and then the percentage of positive cells was calculated. Positive rate (%) is equal to the number of positive cells divided with the total number of cells multiplied with 100. For slices of lymph nodes, because the density and quantity of cells are relatively large, immunohistochemical staining for p-Drp1 was quantified by area density analysis by using Image Pro Plus 6.0 software (Media Cybernetics, Inc., Rockville, MD, USA). The accumulated optical density (IOD) and the area of tissue pixels (area) of each photo are obtained. The area density = IOD/area. Higher area density is representative of the higher positive expression level. The antibodies used in this research are listed in **Supplementary Table 4**.

Statistical analysis

Statistical analyses were performed using GraphPad Prism 7.0 and IBM SPSS Statistics 22.0 software. Data are presented as the mean ± standard deviation (SD) from at least

three independent experiments. Differences between groups were analyzed using an unpaired, two-tailed Student's t-test (for two groups) or one-way analysis of variance (ANOVA) followed by an appropriate post hoc test (for three or more groups). Statistical significance was defined as follows: *$p \leq 0.05$; **$p \leq 0.01$; ***$p \leq 0.001$; ****$p \leq 0.0001$

Results

Mtb infection promotes Drp1 phosphorylation to restrict intracellular bacterial survival in macrophages

To determine whether Mtb infection affects mitochondrial morphology in macrophages, we labeled mitochondria in mouse bone marrow-derived macrophages (BMDMs) with MitoTracker and measured mitochondrial length following infection. We found that mitochondrial length was significantly reduced at 48 hrs post-infection compared to uninfected controls (**Fig. 1A**), suggesting that Mtb infection induces mitochondrial fragmentation. Next, we examined the expression of mitochondrial fission related proteins involves Drp1 (encoded by dynamin 1 like (*Dnm1l*) gene)), mitochondrial fission factor (Mff), fission mitochondrial 1 (Fis1), mitochondrial dynamics protein of 51 kDa (Mid51) (encoded by mitochondrial elongation factor 1 (*Mief1*) gene), mitochondrial dynamics protein of 49 kDa (Mid49) (encoded by mitochondrial elongation factor 2 (*Mief2*) gene). We found that the expression of phosphorylation of Drp1 (p-Drp1), as well as its receptors of Fis1, Mff, Mid49, were significantly upregulated upon Mtb infection for 48 h, whereas the total expression levels of Drp1 and Mid51 remained unchanged (**Fig. 1B**). To further investigate whether these mitochondrial fission-related proteins affect Mtb survival in macrophages, siRNAs targeting their genes have been used to knock down all of these genes in BMDMSs. Efficient knockdown of all target genes was confirmed at both mRNA and protein levels

(**Supplementary Fig. 1A and B**). Intracellular bacterial survival was assessed by CFU assay, which revealed that Drp1 silencing significantly reduced Mtb survival at 48 and 72 h post-infection. In contrast, knockdown of Fis1, Mff, Mid49, or Mid51 did not affect Mtb survival (**Fig. 1C**). Collectively, these results indicate that Drp1 phosphorylation is upregulated upon Mtb infection in macrophages and that Drp1 restricts intracellular Mtb survival.

Drp1 restricts intracellular Mtb survival in macrophages and protects mice from Mtb infection

To further verify the antibacterial function of Drp1 in macrophages, we used siRNA targeting *Dnm1l* in RAW264.7 murine macrophage and confirmed efficient Drp1 knockdown at the protein level (**Fig. 2A**). Drp1 silencing significantly increased bacterial burden upon Mtb infection at 48 hrs (**Fig. 2B**). Consistently, knockdown of Drp1 using two independent short hairpin RNAs (shRNAs) also resulted in a potent reduction of Drp1 expression (**Fig. 2C**) and a corresponding increase in Mtb survival at 48 hrs post-infection (**Fig. 2D**). Conversely, overexpression of Drp1 in RAW264.7 was confirmed by elevated protein levels (**Fig. 2E**) and significantly decreased Mtb survival at 48 hrs post-infection (**Fig. 2F**). We further treated BMDMs with Mdivi-1, a pharmacological inhibitor of Drp1, which decreased Drp1 expression (**Fig. 2G**) and significantly increased Mtb burden at 48 hrs post-infection (**Fig. 2H**). Moreover, Mdivi-1 treatment promoted Mtb survival in the lungs of mice following 4 week and 8 weeks

of Mtb infection **(Supplementary Fig. 2A)**.

To further examine how Drp1 affects Mtb infection in vivo, we generated *Dnm1l*$^{Lyz2\text{-}cre}$ mice with myeloid cell-specific deletion of Drp1 by crossing Dnm1l-floxed mice with Lyz2-Cre mice. Deletion of Drp1 in BMDMs was confirmed by Western blot (**Fig. 2J**). Following infection with Mtb, *Dnm1l*$^{Lyz2\text{-}cre}$ mice exhibited increased Mtb survival in the lungs compared to *Dnm1l*$^{fl/fl}$ control mice (**Fig. 2K**). Along with enhanced bacterial burden, enlarged spleens (Fig. 2L) and increased inflammatory infiltration in the lungs (Fig. 2M) were observed in *Dnm1l*$^{Lyz2\text{-}cre}$ mice. Consistently, we found that production of proinflammatory cytokines including IL-6, TNF-α, and IL-1β was significantly increased, while production of anti-inflammatory cytokine IL-10 was significantly decreased in lungs and spleens of *Dnm1l*$^{Lyz2\text{-}cre}$ mice compared with control mice (**Fig. 2N**). Then, we investigate whether *Dnm1l*$^{Lyz2\text{-}cre}$ knockout show alterations in the myeloid compartment in lungs. The results showed that proportion of inflammatory macrophages has decreased, while the proportion of inflammatory monocytes was not influenced at 4 weeks post infection (**Fig. 2O**). However, *Dnm1l* deletion in macrophages did not affect $CD4^+$ and $CD8^+$ T cell differentiation or M1 and M2 polarization (**Supplementary Fig. 2B and C**). These results indicated that Drp1 functions on macrophages to restrict Mtb survival in the lungs of mice. Mechanistically, Drp1 limits excessive inflammatory responses and promotes macrophage infiltration, thereby controlling bacterial burden. Consistent with this, Drp1 deletion resulted in exacerbated inflammation, elevated pro-inflammatory

561 cytokines, reduced IL-10 production, and impaired macrophage recruitment.

562 **Drp1 restricts Mtb survival by promoting autophagy in macrophages**

563 Drp1 has been reported to affect cell apoptosis and autophagy in regulating various
564 diseases. We found that Drp1 did not influence the expression of caspase-3, a key
565 apoptosis marker, upon Mtb infection in BMDMs (**Supplementary Fig. 3).** To further
566 identify whether Drp1 clears Mtb by promoting selective autophagy, the LC3-II/LC3-I
567 ratio, p62 levels, and other autophagy-related proteins were detected by Western blot
568 analysis. Western blot analysis revealed that Drp1 silencing in BMDMs led to a
569 significant decrease in the LC3-II/LC3-I ratio and Beclin-1 and Atg5 expression, and a
570 concomitant increase in p62 expression at 24 h post Mtb infection; however, Atg7
571 expression was not influenced by Drp1 silencing (**Fig. 3A**). Autophagy induction was
572 further assessed by LC3 puncta formation using microscopy, which revealed that Drp1
573 silencing significantly reduced LC3 puncta, as well as the co-localization of Mtb and
574 LC3, in BMDMs upon Mtb infection (**Fig. 3B**). Consistently, Drp1 knockdown by
575 sh*Dnm1l* resulted in a significant decrease in the LC3-II/LC3-I ratio, Beclin-1 and Atg5
576 expression, and an increase in p62 expression, with no effect on Atg7 (**Fig. 3C**). In
577 RAW264.7 cells, Drp1 knockdown also resulted in a significant reduction in LC3
578 puncta formation and in the co-localization of Mtb and LC3 (Fig. 3D). In contrast, Drp1
579 overexpression led to an increase in the LC3-II/LC3-I ratio and Beclin-1 and Atg5
580 expression, and a decrease in p62 expression, again without affecting Atg7 expression

in Mtb-infected RAW264.7 cells (Fig. 3E). LC3 puncta formation and the co-localization of Mtb and LC3 were significantly enhanced in Drp1-overexpressing RAW264.7 cells (Fig. 3F). Mdivi-1 treatment also inhibited the LC3-II/LC3-I ratio upon Mtb infection at 1, 6 and 24 hrs (**Supplementary Fig. 4**). Additionally, we examined the co-localization of LC3 with the macrophage marker F4/80 in the lungs of mice and found that Dnm1l deletion in macrophages significantly decreased the intensity of co-localization between F4/80 and LC3 (**Fig. 3G**). We further investigated the role of classical autophagy inhibitor 3-methyladenine (3-MA) in regulating Mtb survival in Drp1 overexpressing RAW264.7. The results showed that 3-MA treatment could totally block Drp1 overexpression-induced autophagy formation indicated by LC3-II/LC3-I ratio (**Fig. 3H**). CFU assay further showed that the reduction in Mtb survival conferred by Drp1 overexpression was restored by 3-MA treatment at 48 hrs post Mtb infection (**Fig. 3I**). These results suggest that Drp1 promotes autophagy in macrophages to restrict Mtb survival in macrophages. To rule out the possibility that Drp1-induced autophagy was secondary to mitochondrial damage, we examined mitochondrial membrane potential ($\Delta\Psi m$), mitochondrial ROS production, and mitochondrial DNA copy number. Notably, Drp1 overexpression did not significantly affect any of these parameters in Mtb-infected macrophages (**Supplementary Fig. 5**), suggesting that Drp1 drives xenophagy via a specific signaling axis rather than through global mitochondrial dysfunction. These findings thus prompted us to explore the downstream pathways underlying this protective effect.

HIF-1α is required for Drp1 to promote autophagy to inhibit Mtb survival in macrophages

To identify the downstream effector(s) responsible for Drp1-mediated xenophagy, we first examined several canonical autophagy-regulating pathways. Drp1 silencing did not alter the phosphorylation levels of mTOR or AMPKα in Mtb-infected macrophages (**Supplementary Fig. 6**), excluding the involvement of these two pathways. Given that Parkin has been reported to interact with Drp1 and to modulate intracellular bacterial survival in certain contexts, we next asked whether Parkin acts as a downstream mediator of Drp1. We found Drp1 silencing significantly decreased Parkin expression in both BMDMs and RAW264.7 cells upon Mtb infection (**Supplementary Fig. 7A, B**), whereas Drp1 overexpression increased Parkin expression (**Supplementary Fig. 7C**). To functionally test the requirement of Parkin, we generated Parkin-overexpressing RAW264.7 cells (**Supplementary Fig. 7D**). However, Parkin overexpression failed to reverse the Drp1 silencing-induced reduction in the LC3-II/LC3-I ratio (**Supplementary Fig. 7E**), the decrease in LC3 puncta formation, or the impaired colocalization between Mtb and LC3 (**Supplementary Fig. 7F**). Consistently, Parkin overexpression did not rescue the increased bacterial burden caused by Drp1 silencing (**Supplementary Fig. 7G**). Collectively, these results indicate that Parkin is not a critical downstream effector of Drp1 in promoting xenophagy against Mtb.

Having ruled out mTOR, AMPK, and Parkin as downstream effectors of Drp1-

622 driven xenophagy, we next examined whether HIF-1α mediates this process. The results
623 showed that knockdown of Drp1 by siRNA in RAW264.7 cells or by shRNA in
624 BMDMs significantly reduced HIF-1α protein levels upon Mtb infection for 24 hrs,
625 whereas Drp1 overexpression markedly increased HIF-1α expression **(Fig. 4A-C**). We
626 next asked whether HIF-1α is functionally required for Drp1-mediated autophagy. To
627 this end, we treated Drp1-silenced macrophages with Roxadustat (FG-4592), a prolyl
628 hydroxylase inhibitor that stabilizes HIF-1α. Remarkably, Roxadustat treatment not
629 only restored HIF-1α expression but also rescued the reduction in the LC3-II/LC3-I
630 ratio caused by Drp1 silencing in Mtb-infected macrophages (**Fig. 4D**). Consistently,
631 confocal microscopy revealed that Roxadustat reversed the Drp1 silencing-induced
632 decrease in LC3 puncta formation and the impaired colocalization between LC3 and
633 Mtb (**Fig. 4E**). Furthermore, CFU assays showed that Roxadustat treatment
634 significantly blocked the increased Mtb survival conferred by Drp1 silencing at 48 hrs
635 post-infection (**Fig. 4F**). Collectively, these results demonstrate that Drp1 promotes
636 xenophagy through the HIF-1α pathway to restrict Mtb survival in macrophages.

637 **Drp1 enhances ROS-mediated HIF-1α signaling and autophagic clearance of Mtb**
638 **in macrophages**

639 Previous studies have established that reactive nitrogen species (RNS) and reactive
640 oxygen species (ROS), which are rapidly generated in macrophages upon recognition
641 of invading bacteria, serve as positive effector mechanisms for killing intracellular Mtb

642 [14]. In particular, ROS promotes the recruitment of LC3 to the phagosome, thereby
643 facilitating phagosome–lysosome fusion [15]. Moreover, ROS has been identified as an
644 upstream activator of the HIF-1α pathway, which is closely linked to autophagy
645 induction [16]. Based on these findings, we next investigated whether Drp1 regulates
646 autophagy through ROS- or NO-dependent mechanisms by measuring ROS and NO
647 production in Drp1-manipulated macrophages following Mtb infection. Western blot
648 assay showed that Drp1 silencing reduced iNOS protein expression and NO production
649 in BMDMs at 24 hrs post-infection (**Fig. 5A and B**), and flow cytometry analysis
650 revealed that Drp1 silencing significantly decreased ROS production (**Fig. 5C**).
651 Consistently, shRNA-mediated knockdown of Drp1 in RAW264.7 cells significantly
652 reduced iNOS expression, as well as NO and ROS production at 24 hrs of Mtb infection
653 **(Fig. 5D-F**). In contrast, overexpression of Drp1 significantly increased iNOS
654 expression, NO production, and ROS production in RAW264.7 cells (**Fig. 5G-I**). We
655 next asked whether ROS and NO are involved in autophagy formation mediated by the
656 Drp1-HIF-1α axis to regulate Mtb survival. To this end, we treated Drp1-
657 overexpressing RAW264.7 cells with the NO inhibitor L-NAME during Mtb infection.
658 L-NAME treatment effectively inhibited NO production but did not affect ROS
659 production enhanced by Drp1 overexpression (**Fig. 5J and K**). Moreover, L-NAME
660 treatment failed to reverse the reduced Mtb survival conferred by Drp1 overexpression
661 (**Fig. 5L**), indicating that Drp1 inhibits Mtb survival independently of NO production.
662 We then examined the role of ROS using the potent antioxidant N-acetyl-L-cysteine

(NAC) in Drp1-overexpressing RAW264.7 cells. NAC treatment did not suppress NO production induced by Drp1 overexpression, but it effectively blocked ROS production (**Fig. 5M and N**). CFU assay showed that NAC treatment restored Mtb survival that had been inhibited by Drp1 overexpression at 48 hrs post-infection (**Fig. 5O**). Furthermore, NAC treatment abolished the induction of HIF-1α expression and autophagy, as indicated by the conversion of LC3-I to LC3-II, without affecting iNOS expression (**Fig. 5P**). Collectively, these data indicate that Drp1-mediated suppression of Mtb survival relies on its ability to induce ROS production, which subsequently promotes HIF-1α-dependent autophagy, rather than on NO pathways.

Drp1 promotes ROS-dependent autophagic flux to restrict Mtb survival in macrophages

To confirm that this pathway represents productive autophagic flux rather than autophagosome accumulation, we treated Drp1-overexpressing macrophages with chloroquine (CQ), which blocks autophagosome-lysosome fusion by neutralizing lysosomal pH. CQ treatment further increased LC3-II and p62 accumulation in Drp1-overexpressing cells (**Fig. 6A**) and reversed the reduction in Mtb survival conferred by Drp1 overexpression (**Fig. 6B**). These results indicate that Drp1 enhances functional autophagic degradation of intracellular Mtb. To determine whether the autophagy defect caused by Drp1 deficiency could be rescued by an independent autophagy stimulus, we treated Drp1-silenced macrophages with CCCP, a

683 well-established inducer of autophagy that triggers autophagosome formation through
684 ROS-dependent pathways [17]. Western blot analysis showed that Drp1 silencing
685 reduced the LC3-II/LC3-I ratio, whereas CCCP treatment reversed this reduction (**Fig.**
686 **6C**). Confocal microscopy further revealed that Drp1 silencing significantly decreased
687 LC3 puncta formation and the colocalization of LC3 with mCherry-labeled Mtb, CCCP
688 treatment alone increased LC3 puncta and restored both LC3 puncta and Mtb-LC3
689 colocalization in Drp1-silenced cells (**Fig. 6D**). When determining the changes in
690 cellular autophagy activity, it is necessary to evaluate the changes in the autophagy flux.
691 The cells engulf autophagic substances into autophagosomes until the autolysosome
692 forms and degrade the autophagic substances. This process is called autophagy flux.
693 The fusion protein that can detect the level of autophagy flux uses the tandem
694 fluorescent proteins mCherry (red light)-eGFP (green light)-LC3. It utilizes the pH
695 difference between acidic autolysosomes and neutral autophagosomes, as well as the
696 differences in the sensitivity of different fluorescent dyes to pH, to monitor the process
697 from autophagosomes to autolysosomes. To detect whether Drp1 affects the activation
698 of autophagic flux, we constructed a mCherry-eGFP-LC3 dual-fluorescence reporter of
699 autophagic flux system in RAW264.7 cells. Drp1 silencing reduced both the yellow
700 fluorescence and the red fluorescence significantly, indicating that Drp1 silencing can
701 inhibit the level of autophagic flux upon Mtb infection, and CCCP treatment restored
702 the level of autophagic flux inhibited by Drp1 **(Fig. 6E)**. Moreover, CCCP treatment
703 increased ROS production and reversed the reduction in ROS levels caused by Drp1

704 silencing in Mtb-infected BMDMs (**Fig. 6F**). Functionally, CCCP treatment
705 significantly reduced the increased Mtb survival in Drp1-silenced macrophages (**Fig.**
706 **6G**). Collectively, these results indicate that Drp1 promotes
707 ROS-HIF-1α-axis-mediated autophagic flux to restrict Mtb survival in macrophages.

708 **Drp1 phosphorylation at Ser616 is required for ROS-dependent autophagic flux**
709 **and xenophagic clearance of Mtb**

710 To evaluate the translational relevance of Drp1 phosphorylation at Ser616, we
711 examined its expression in tissue specimens from six independent patients with
712 tuberculosis. Immunohistochemical analysis revealed that p-Drp1 (S616) levels were
713 significantly elevated in both lymphocyte and lung tissue samples from TB patients
714 compared with control tissues from patients with chronic inflammation (**Fig. 7A**),
715 suggesting that Ser616 phosphorylation is associated with human tuberculosis
716 pathology.

717 To determine whether these effects depend on phosphorylation of Drp1 at Ser616,
718 we generated RAW264.7 macrophages stably expressing a phosphorylation-deficient
719 mutant (S616A) of Drp1. Overexpression of wild-type Drp1 (Drp1-Wt) led to a marked
720 increase in Ser616 phosphorylation, whereas the S616A mutant showed a substantial
721 reduction in phosphorylation at this site, which was barely detectable, despite
722 comparable total Drp1 protein levels (**Fig. 7B**). Notably, S616A expression did not
723 cause overt mitochondrial dysfunction, as assessed by ΔΨm, mtROS, and mtDNA copy

number (**Supplementary Fig. 5**), allowing us to attribute downstream effects specifically to the loss of phosphorylation. Consistently, Drp1-WT upregulated HIF-1α expression and promoted autophagic flux as indicated by the LC3-II/LC3-I ratio and p62 degradation, whereas the S616A mutant exhibited markedly reduced HIF-1α expression and impaired autophagic flux (**Fig. 7B**). Furthermore, confocal microscopy analysis demonstrated that overexpression of Drp1-Wt markedly promoted the colocalization of Mtb with LAMP1, indicating enhanced delivery of bacteria to lysosomes. Consistently, a significant increase in p62-Mtb colocalization was also observed under Drp1-Wt overexpression, suggesting the activation of selective autophagy targeting the pathogen. Notably, all these effects were largely abrogated in macrophages expressing the S616A mutant, as both the LAMP1-Mtb and p62-Mtb colocalization signals reverted to low levels, phenocopying the control group (**Fig. 7C and D**). These results collectively indicate that Drp1-mediated autophagic clearance of Mtb is strictly dependent on the phosphorylation of Ser616. We next examined whether S616A mutation affects the downstream signaling mediated by Drp1. In contrast to Drp1-WT, which markedly enhanced ROS production, the S616A mutant failed to elevate ROS levels under the same conditions (**Fig. 7E**). Drp1-WT significantly restricted intracellular Mtb survival, whereas the S616A mutant failed to reduce Mtb burdens, remaining comparable to control cells (**Fig. 7F**).

Collectively, these results demonstrate that Drp1 phosphorylation at Ser616 is essential for ROS production, HIF-1α stabilization, autophagic flux, and lysosomal

delivery of Mtb, thereby restricting intracellular bacterial survival. The S616A mutant was defective in all these processes, identifying Ser616 phosphorylation as a critical upstream switch for the ROS–HIF-1α–autophagy axis in macrophage anti-tuberculosis immunity. A schematic model summarizing this pathway is presented in Fig. 8.

Discussion

Macrophages activate antibacterial gene expression through multiple extracellular and intracellular pattern-recognition receptor pathways. They can also initiate innate immune responses by detecting mitochondrial damage-derived components in the cytoplasm, such as mitochondrial fragments, mitochondrial DNA (mtDNA), and mitochondrial RNA (mtRNA). Growing evidence across various disease models indicates that mitochondrial dysfunction and the release of mitochondrial damage-associated molecular patterns (mito-DAMPs) can potentiate innate immunity and increase host susceptibility to pathogens. For instance, mtDNA in macrophages has been shown to promote inflammasome activation[18], while mitochondrial double-stranded RNA can stimulate the MDA5-dependent interferon signaling pathway, enhancing antiviral immunity[19]. Additionally, the mitochondrial protein ERAL1 interacts with MAVS, leading to MAVS activation and RIG-I/MDA5 ubiquitination, thereby promoting RIG-I-like receptor (RLR)-mediated antiviral responses[5].Notably, mitochondrial damage mechanisms and Mtb infection have been reported to activate overlapping innate immune pathways[3]. Therefore, leveraging the multifaceted signaling functions of mitochondria represents a promising strategy for modulating the

766 immune response against Mtb infection.

767 Mitochondrial fusion and fission proteins play crucial roles in maintaining
768 cellular physiology and regulating host defense mechanisms, particularly against viral
769 infection. For example, during RNA viral infection, Drp1-dependent mitochondrial
770 fission has been shown to inhibit MAVS-mediated RLR signaling and the subsequent
771 antiviral immune response[20]. Proteins such as MiD49 and MiD51 promote Drp1-
772 mediated fission, which can inhibit apoptosis and exacerbate conditions like pulmonary
773 arterial hypertension[21]. Conversely, the fusion protein Mfn2 interacts with MAVS to
774 suppress the activation of RIG-I, MDA5, IRF-3, and NF-κB, thereby inhibiting IFN-β
775 production and viral replication[22]. Mfn1, in contrast, forms a complex with STING
776 and MAVS that dissociates upon RLR activation, facilitating TBK1 recruitment and
777 promoting interferon signaling[23]. Other proteins like OPA-1 support immune
778 function by enhancing mitochondrial complex I activity and neutrophil extracellular
779 trap formation against bacterial infection[24], while the fission factor Mff promotes
780 MAVS aggregation on mitochondria to potentiate antiviral responses[25]. Recent
781 research has extended this paradigm to bacterial infection, revealing that the
782 mitochondrial fusion protein Mfn2 is critical for innate immune regulation during Mtb
783 infection. Mfn2 promotes NLRP3 inflammasome activation and IL-1β secretion[7] ,
784 drives ROS production and autophagy for bacterial clearance[26], and sustains HIF-1α-
785 mediated aerobic glycolysis and autophagy in infected macrophages[6]. In contrast, the
786 role of mitochondrial fission proteins during Mtb infection remains largely

uncharacterized. Here, we report that Mtb infection induces mitochondrial fragmentation in macrophages and increases Drp1 phosphorylation at Ser616 both in vitro and in tissue samples from patients with lymph node and pulmonary tuberculosis. Using siRNA-mediated knockdown of key fission proteins—Fis1, Mff, MiD49, MiD51, and Drp1—we found that only depletion of Drp1 significantly reduced intracellular Mtb survival in macrophages, as measured by CFU assay. This identifies Drp1 as a specific and essential fission-related regulator of host defense against Mtb.

Drp1 plays a crucial regulatory role in numerous immune and cellular processes, including T cell function, macrophage polarization, inflammatory cytokine production, apoptosis, and autophagy, and has emerged as a therapeutic target for modulating adaptive immunity[27]. For instance, in hepatocellular carcinoma, sustained Drp1 activation via mTOR signaling suppresses mitochondrial metabolism, enabling tumor cells to evade NK cell-mediated killing, a mechanism that suggests targeting Drp1 could enhance NK cell-based cancer therapies[28]. In atherosclerosis, the Drp1 inhibitor Mdivi-1 attenuates disease progression by blocking Drp1-dependent mitochondrial fission, thereby reducing M1 macrophage polarization and NLRP3 inflammasome activation mediated by mitochondrial ROS[29]. Furthermore, Drp1 influences inflammatory signaling through multiple pathways: in LPS-stimulated macrophages, Drp1 activation enhances mitochondrial ATP synthesis and promotes TNF-α and IL-6 production via ROS/NF-κB signaling [30]. In alveolar macrophages, Drp1-driven mitochondrial fission and ROS release bolster NLRP3-mediated IL-1β

808 production, which restricts influenza virus infection[31]. In cancer contexts, Drp1 can
809 facilitate tumor growth by opening the mitochondrial permeability transition pore
810 (mPTP), inducing mtDNA stress, and activating the cGAS-STING pathway to promote
811 autophagy[12]. Conversely, Drp1 silencing impairs mitochondrial fission and
812 mitophagy, shifting cells toward glycolysis, reducing ATP output, and increasing
813 susceptibility to apoptosis during HCV infection[32]. Drp1 is also essential for
814 development, as its deficiency disrupts mitophagy and calcium homeostasis, impairing
815 muscle formation and causing lethality in mice[33]. Additionally, in cerebral ischemia-
816 reperfusion injury, Drp1 accelerates p62-mediated autophagy while inhibiting
817 autophagosome-lysosome fusion via the RIP1/RIP3 pathway, ultimately reducing
818 tissue damage[34]. Given that these immune and cellular processes are central to the
819 host response against Mtb, we investigated whether Drp1 influences anti-tuberculosis
820 immunity through similar mechanisms. In this study, we observed that myeloid-specific
821 Drp1 knockout (Drp1 cKO) mice exhibited significantly increased spleen weight,
822 heightened inflammatory infiltration in the lungs, and elevated pulmonary TNF-α levels
823 following Mtb infection, likely reflecting aggravated infection and enhanced cytokine
824 secretion. However, the proportions of differentiated $CD4^+$ and $CD8^+$ T cell subsets,
825 monocytes, and overall macrophage polarization remained unchanged, though the
826 proportion of inflammatory macrophages in the lungs was reduced. Furthermore, Drp1
827 silencing in Mtb-infected macrophages did not alter the expression of cleaved caspase-
828 3, indicating that apoptosis was not affected. These findings suggest that Drp1 does not

829 modulate the anti-Mtb immune response via T cell function, macrophage polarization,
830 inflammatory cytokine production, or apoptosis. Further investigation revealed that the
831 co-localization of the macrophage marker F4/80 with the autophagy marker LC3 was
832 significantly increased in the lungs of infected Drp1 cKO mice. In vitro, Drp1 promoted
833 the expression of autophagy-related proteins LC3-II, Beclin-1, and Atg5 in Mtb-
834 infected macrophages and enhanced the co-localization of LC3-II with intracellular
835 bacteria. However, while Drp1 overexpression enhanced the recruitment of LAMP1-
836 positive lysosomes to Mtb-containing compartments, it also significantly increased the
837 co-localization of p62 with Mtb, suggesting that although autophagosome-lysosome
838 fusion was promoted, the selective sequestration of bacteria into autophagosomes was
839 concomitantly enhanced. Importantly, the classical autophagy inhibitor 3-MA reversed
840 both the elevated autophagy and the restriction of Mtb survival induced by Drp1
841 overexpression. Collectively, these results indicate that Drp1 inhibits Mtb infection
842 primarily by promoting autophagy in macrophages.

843 Following infection of host macrophages by Mtb, the induction of autophagy
844 leads to the fusion of Mtb-containing phagosomes with lysosomes, a key mechanism
845 by which the host combats the pathogen. Autophagy is a multi-step cascade mediated
846 by a suite of autophagy-related (Atg) proteins. During initiation, vacuole membrane
847 protein 1 (VMP1) interacts with the Beclin1 and ULK1 complex to nucleate
848 autophagosome formation. The Atg12-Atg5 conjugate, facilitated by Atg7, plays a
849 crucial role in the final expansion stage, promoting the conversion of cytosolic

microtubule-associated protein 1A/1B-light chain 3 (LC3-I) to its phosphatidylethanolamine (PE)-conjugated form, LC3-II. LC3-II becomes embedded in the elongating autophagosomal membrane, and its punctate distribution serves as a hallmark of active autophagosome formation[35]. Beyond its role in degrading cellular components, autophagy machinery directly participates in anti-mycobacterial immunity. Proteins such as Beclin1, Atg5, and Atg7 are essential for the autophagic control of Mtb[36]. This process is often regulated by key signaling nodes. For example, IL-36γ promotes autophagy and host defense via the COX-2/AKT/mTOR axis[37], and the RNA sensor ZNFX1 sustains autophagy flux by stabilizing AMPK mRNA[38]. AMPK activation itself inhibits mTOR, thereby promoting oxidative phosphorylation and autophagy protein synthesis to restrict Mtb[39], making the AMPK/mTOR pathway a recognized therapeutic target[40]. Notably, AMPK and mTOR also intersect with mitochondrial dynamics, regulating fusion and fission in various disease contexts[41]. A critical step in targeting intracellular Mtb for autophagy (xenophagy) is its labeling with ubiquitin, which is recognized by adaptor proteins like p62 to envelope the bacterium within an autophagosome. Several E3 ubiquitin ligases mediate this process. Smurf1 promotes K48-linked ubiquitination of Mtb and autophagic clearance in mice[42], and UBQLN1 facilitates IFN-γ-induced xenophagy independently of Parkin[43]. Parkin, a well-characterized E3 ubiquitin ligase, mediates K63-linked ubiquitination of multiple substrates and plays a critical role in the autophagic clearance of Mtb[44]. Given that Drp1 has been reported to regulate Parkin expression and

activation in various cellular contexts[45], we reasoned that Parkin might act as a downstream effector of Drp1 to orchestrate xenophagic clearance of Mtb. In this study, we first determined that Drp1 does not influence the activation status of AMPK or mTOR in Mtb-infected macrophages, indicating that its pro-autophagic effect is independent of these canonical pathways. We then examined whether Parkin mediates the autophagy-promoting function of Drp1. Although Drp1 positively regulated Parkin expression in infected macrophages, forced expression of Parkin failed to reverse the autophagy defect or the increased bacterial burden caused by Drp1 deficiency, indicating that Parkin is not the key downstream mediator of Drp1 in this context. To further dissect the mechanistic basis of Drp1-mediated autophagy, we next asked whether the pro-autophagic function of Drp1 requires its phosphorylation at Ser616. Using a phosphorylation-deficient S616A mutant, we found that this mutant failed to promote LC3-II expression, autophagosome formation, and autophagic clearance of Mtb, phenocopying the effects of Drp1 knockdown. This establishes that Ser616 phosphorylation of Drp1 is the essential molecular switch that activates xenophagy in macrophages. Concurrently, we assessed whether Drp1 mediated autophagy was associated with alterations in mitochondrial function. Notably, Drp1 manipulation did not significantly affect mitochondrial membrane potential, mitochondrial reactive oxygen species (mtROS) production, or mitochondrial DNA (mtDNA) copy number in Mtb-infected macrophages, suggesting that the pro-autophagic function of Drp1 operates independently of global mitochondrial homeostasis.

892 The production of intracellular reactive oxygen species (ROS) serves as both a
893 critical bactericidal mechanism and a key signaling molecule for sustaining autophagy
894 in macrophages during Mtb infection. Previous studies have implicated Drp1 in
895 modulating cellular ROS levels. For example, in cerebral ischemia-reperfusion injury,
896 inhibiting Thrombospondin-1 (Thbs-1) prevents Drp1-mediated mitochondrial fission
897 and subsequent ROS generation, thereby reducing cardiomyocyte damage[46].
898 Additionally, various Drp1 inhibitors can alleviate neuropathic pain by correcting ROS
899 homeostasis through distinct mechanisms[47], though the precise molecular pathways
900 remain incompletely defined. Notably, ROS is a well-established inducer of the
901 transcription factor HIF-1α[48], which promotes autophagy, cytokine release, and
902 mycobactericidal activity in Mtb-infected macrophages[49]. Furthermore, the HIF-
903 1α/BNIP3/Beclin-1 axis is essential for lactate-induced autophagy under hypoxic
904 conditions[50]. Our results demonstrate that Drp1 promotes ROS production and
905 enhances HIF-1α expression in Mtb-infected macrophages. Specifically, wild-type
906 Drp1 overexpression increased ROS levels and HIF-1α expression, whereas the
907 phosphorylation-deficient S616A mutant failed to do so, indicating that Ser616
908 phosphorylation is required for Drp1-driven ROS generation. Mechanistically, the ROS
909 inhibitor N-acetylcysteine (NAC) reduced ROS levels and correspondingly attenuated
910 the elevated HIF-1α expression and autophagy in Drp1-overexpressing macrophages.
911 Conversely, the HIF-1α agonist Roxadustat restored autophagy and restricted Mtb
912 survival in Drp1-silenced cells. Moreover, the mitochondrial uncoupler CCCP (an

autophagy inducer) rescued ROS production, autophagosome formation, and autophagic flux in Drp1-silenced macrophages, leading to inhibited bacterial growth. Additionally, to address a potential concern regarding the use of the pharmacological Drp1 inhibitor Mdivi-1, which has been reported to inhibit mitochondrial complex I independently of Drp1 and could thus confound metabolic interpretations, we validated our key findings using genetic Drp1 knockdown. The consistency between the inhibitor-based and genetic approaches supports that our primary conclusions are not solely driven by off-target effects. Collectively, these findings establish that Drp1 drives protective autophagy through a phosphorylation-dependent ROS–HIF-1α signaling axis, though the specific downstream effectors of this pathway warrant further investigation.

Based on our findings, we establish Drp1-mediated mitochondrial fission as a critical regulator of innate immune defense against Mtb. Mechanistically, Mtb infection triggers Drp1 phosphorylation at Ser616, which serves as an essential molecular switch that activates a ROS–HIF-1α signaling axis to promote xenophagic clearance of Mtb in macrophages (**Fig. 8**). Notably, this phosphorylation-dependent function of Drp1 operates independently of mitochondrial fragmentation or global mitochondrial dysfunction, indicating a non-canonical role for Drp1 in anti-mycobacterial immunity. Collectively, our findings demonstrate that Drp1 plays a protective role against Mtb infection by enhancing xenophagic clearance in macrophages, highlighting the therapeutic potential of targeting Drp1 for host-directed anti-tuberculosis interventions.

References

1. Trajman A, Campbell JR, Kunor T, et al. Tuberculosis. Lancet. 2025; 405(10481): 850-66.

2. Russell DG, Simwela NV, Mattila JT, et al. How macrophage heterogeneity affects tuberculosis disease and therapy. Nat Rev Immunol. 2025; 25(5): 370-84.

3. Patrick KL, Watson RO. Mitochondria: Powering the Innate Immune Response to Mycobacterium tuberculosis Infection. Infect Immun. 2021; 89(4).

4. Chan DC. Mitochondrial Dynamics and Its Involvement in Disease. Annu Rev Pathol. 2020; 15: 235-59.

5. Li S, Kuang M, Chen L, et al. The mitochondrial protein ERAL1 suppresses RNA virus infection by facilitating RIG-I-like receptor signaling. Cell Rep. 2021; 34(3): 108631.

6. Silwal P, Kim JK, Jeon SM, et al. Mitofusin-2 boosts innate immunity through the maintenance of aerobic glycolysis and activation of xenophagy in mice. Commun Biol. 2021; 4(1): 548.

7. Xu F, Qi H, Li J, et al. Mycobacterium tuberculosis infection up-regulates MFN2 expression to promote NLRP3 inflammasome formation. J Biol Chem. 2020; 295(51): 17684-97.

8. Lin AJ, Joshi AU, Mukherjee R, et al. deltaPKC-Mediated DRP1 Phosphorylation Impacts Macrophage Mitochondrial Function and Inflammatory Response to Endotoxin. Shock. 2022; 57(3): 435-43.

9. Jin J, Yan P, Wang D, et al. Targeting lactylation reinforces NK cell cytotoxicity within the tumor microenvironment. Nat Immunol. 2025; 26(7): 1099-112.

10. Simula L, Campanella M, Campello S. Targeting Drp1 and mitochondrial fission for therapeutic immune modulation. Pharmacol Res. 2019; 146: 104317.

11. Fan RZ, Sportelli C, Lai Y, et al. A partial Drp1 knockout improves autophagy flux independent of mitochondrial function. Mol Neurodegener. 2024; 19(1): 26.

12. Li Y, Chen H, Yang Q, et al. Increased Drp1 promotes autophagy and ESCC progression by mtDNA stress mediated cGAS-STING pathway. J Exp Clin Cancer Res. 2022; 41(1): 76.

13. Yuan YJ, Chen T, Yang YL, et al. E2F1/CDK5/DRP1 axis mediates microglial mitochondrial division and autophagy in the pathogenesis of cerebral ischemia-reperfusion injury. Clin Transl Med. 2025; 15(2): e70197.

14. Dharmaraja AT. Role of Reactive Oxygen Species (ROS) in Therapeutics and Drug Resistance in Cancer and Bacteria. J Med Chem. 2017; 60(8): 3221-40.

15. Huang J, Lam GY, Brumell JH. Autophagy signaling through reactive oxygen species. Antioxid Redox Signal. 2011; 14(11): 2215-31.

16. Song K, Li B, Chen YY, et al. LRPPRC regulates metastasis and glycolysis by modulating autophagy and the ROS/HIF1-alpha pathway in retinoblastoma. Mol Ther Oncolytics. 2021; 22: 582-91.

17. Kwon KY, Viollet B, Yoo OJ. CCCP induces autophagy in an AMPK-independent manner. Biochem Biophys Res Commun. 2011; 416(3-4): 343-8.

18. Lewis Lujan LM, McCarty MF, Di Nicolantonio JJ, et al. Nutraceuticals/Drugs Promoting Mitophagy and Mitochondrial Biogenesis May Combat the Mitochondrial Dysfunction Driving Progression of Dry Age-Related Macular Degeneration. Nutrients. 2022; 14(9).

19. Dhir A, Dhir S, Borowski LS, et al. Mitochondrial double-stranded RNA triggers antiviral signalling in humans. Nature. 2018; 560(7717): 238-42.

20. Yasukawa K, Kinoshita D, Yaku K, et al. The microRNAs miR-302b and miR-372 regulate mitochondrial metabolism via the SLC25A12 transporter, which controls MAVS-mediated antiviral innate immunity. J Biol Chem. 2020; 295(2): 444-57.

21. Chen KH, Dasgupta A, Lin J, et al. Epigenetic Dysregulation of the Dynamin-Related Protein 1 Binding Partners MiD49 and MiD51 Increases Mitotic Mitochondrial Fission and Promotes Pulmonary Arterial Hypertension: Mechanistic and Therapeutic Implications. Circulation. 2018; 138(3): 287-304.

22. Luo Z, Liu LF, Jiang YN, et al. Novel insights into stress-induced susceptibility to influenza: corticosterone impacts interferon-beta responses by Mfn2-mediated ubiquitin degradation of MAVS. Signal Transduct Target Ther. 2020; 5(1): 202.

23. Brubaker SW, Gauthier AE, Mills EW, et al. A bicistronic MAVS transcript highlights a class of truncated variants in antiviral immunity. Cell. 2014; 156(4): 800-11.

24. Amini P, Stojkov D, Felser A, et al. Neutrophil extracellular trap formation requires OPA1-dependent glycolytic ATP production. Nat Commun. 2018; 9(1): 2958.

997 25. Hanada Y, Ishihara N, Wang L, et al. MAVS is energized by Mff which senses
998 mitochondrial metabolism via AMPK for acute antiviral immunity. Nat Commun. 2020;
999 11(1): 5711.
1000 26. Tur J, Pereira-Lopes S, Vico T, et al. Mitofusin 2 in Macrophages Links
1001 Mitochondrial ROS Production, Cytokine Release, Phagocytosis, Autophagy, and
1002 Bactericidal Activity. Cell Rep. 2020; 32(8): 108079.
1003 27. Liu S, Huang Z, Yin Z, et al. Drp1 in Parkinson's disease: Mechanisms of disease
1004 pathology and the promise of targeted therapeutic strategies. Life Sci. 2026; 384:
1005 124086.
1006 28. Zheng X, Qian Y, Fu B, et al. Mitochondrial fragmentation limits NK cell-based
1007 tumor immunosurveillance. Nat Immunol. 2019; 20(12): 1656-67.
1008 29. Su ZD, Li CQ, Wang HW, et al. Inhibition of DRP1-dependent mitochondrial
1009 fission by Mdivi-1 alleviates atherosclerosis through the modulation of M1 polarization.
1010 J Transl Med. 2023; 21(1): 427.
1011 30. Yu W, Wang X, Zhao J, et al. Stat2-Drp1 mediated mitochondrial mass increase is
1012 necessary for pro-inflammatory differentiation of macrophages. Redox Biol. 2020; 37:
1013 101761.
1014 31. Park HS, Liu G, Liu Q, et al. Swine Influenza Virus Induces RIPK1/DRP1-
1015 Mediated Interleukin-1 Beta Production. Viruses. 2018; 10(8).
1016 32. Kim SJ, Syed GH, Khan M, et al. Hepatitis C virus triggers mitochondrial fission
1017 and attenuates apoptosis to promote viral persistence. Proc Natl Acad Sci U S A. 2014;

1018 111(17): 6413-8.
1019 33. Favaro G, Romanello V, Varanita T, et al. DRP1-mediated mitochondrial shape
1020 controls calcium homeostasis and muscle mass. Nat Commun. 2019; 10(1): 2576.
1021 34. Zeng X, Zhang YD, Ma RY, et al. Activated Drp1 regulates p62-mediated
1022 autophagic flux and aggravates inflammation in cerebral ischemia-reperfusion via the
1023 ROS-RIP1/RIP3-exosome axis. Mil Med Res. 2022; 9(1): 25.
1024 35. Mizushima N, Komatsu M. Autophagy: renovation of cells and tissues. Cell. 2011;
1025 147(4): 728-41.
1026 36. Pahari S, Negi S, Aqdas M, et al. Induction of autophagy through CLEC4E in
1027 combination with TLR4: an innovative strategy to restrict the survival of
1028 Mycobacterium tuberculosis. Autophagy. 2020; 16(6): 1021-43.
1029 37. Gao Y, Wen Q, Hu S, et al. IL-36gamma Promotes Killing of Mycobacterium
1030 tuberculosis by Macrophages via WNT5A-Induced Noncanonical WNT Signaling. J
1031 Immunol. 2019; 203(4): 922-35.
1032 38. Liu H, Han Z, Chen L, et al. ZNFX1 promotes AMPK-mediated autophagy against
1033 Mycobacterium tuberculosis by stabilizing Prkaa2 mRNA. JCI Insight. 2024; 9(1).
1034 39. Yang CS, Kim JJ, Lee HM, et al. The AMPK-PPARGC1A pathway is required for
1035 antimicrobial host defense through activation of autophagy. Autophagy. 2014; 10(5):
1036 785-802.
1037 40. Cerni S, Shafer D, To K, et al. Investigating the Role of Everolimus in mTOR
1038 Inhibition and Autophagy Promotion as a Potential Host-Directed Therapeutic Target

in Mycobacterium tuberculosis Infection. J Clin Med. 2019; 8(2).

41. Lopez-Lluch G. Mitochondrial activity and dynamics changes regarding metabolism in ageing and obesity. Mech Ageing Dev. 2017; 162: 108-21.

42. Franco LH, Nair VR, Scharn CR, et al. The Ubiquitin Ligase Smurf1 Functions in Selective Autophagy of Mycobacterium tuberculosis and Anti-tuberculous Host Defense. Cell Host Microbe. 2017; 21(1): 59-72.

43. Sakowski ET, Koster S, Portal Celhay C, et al. Ubiquilin 1 Promotes IFN-gamma-Induced Xenophagy of Mycobacterium tuberculosis. PLoS Pathog. 2015; 11(7): e1005076.

44. Manzanillo PS, Ayres JS, Watson RO, et al. The ubiquitin ligase parkin mediates resistance to intracellular pathogens. Nature. 2013; 501(7468): 512-6.

45. Krzystek TJ, Banerjee R, Thurston L, et al. Differential mitochondrial roles for alpha-synuclein in DRP1-dependent fission and PINK1/Parkin-mediated oxidation. Cell Death Dis. 2021; 12(9): 796.

46. Kelm NQ, Beare JE, Weber GJ, et al. Thrombospondin-1 mediates Drp-1 signaling following ischemia reperfusion in the aging heart. FASEB Bioadv. 2020; 2(5): 304-14.

47. Dai CQ, Guo Y, Chu XY. Neuropathic Pain: the Dysfunction of Drp1, Mitochondria, and ROS Homeostasis. Neurotox Res. 2020; 38(3): 553-63.

48. Belaidi E, Morand J, Gras E, et al. Targeting the ROS-HIF-1-endothelin axis as a therapeutic approach for the treatment of obstructive sleep apnea-related cardiovascular complications. Pharmacol Ther. 2016; 168: 1-11.

49. Li Q, Xie Y, Cui Z, et al. Activation of hypoxia-inducible factor 1 (Hif-1) enhanced bactericidal effects of macrophages to Mycobacterium tuberculosis. Tuberculosis (Edinb). 2021; 126: 102044.

50. Pan Y, Wu G, Chen M, et al. Lactate Promotes Hypoxic Granulosa Cells' Autophagy by Activating the HIF-1alpha/BNIP3/Beclin-1 Signaling Axis. Genes (Basel). 2024; 16(1).

Statements

Statement of Ethics

This study protocol was reviewed and approved by Ethics Committee of the Southern Medical University.

Conflict of Interest Statement

The authors have no conflicts of interest to declare.

Funding Sources

This work was supported by Major Project of Guangzhou National Laboratory (GZNL2024A01023), Prevention and Control of Emerging and Major Infectious Diseases-National Science and Technology Major Project (2025ZD01907200), National Natural Science Foundation of China (82470013, 82272344, 82472303), Guangdong Basic and Applied Basic Research Foundation (2024A1515013089, 2024A1515011320, 2025A1515012373). Provincial Key Laboratory of Immune Regulation and Immunotherapy (2022B1212010009).

Author Contributions

Qianna Li, Qi Wang, Binchi Mo: acquisition of data, analysis and interpretation of data, drafting of the manuscript, statistical analysis and critical revision of the manuscript; **Bo Zhu**: acquisition of data, analysis and interpretation of data, drafting of the manuscript, **Lingming Lin, Hongxuan Li, Jintang He, Shou Chen, Zhenyu Han and Minna Xu**: contributed to acquisition of data. **Qian Wen, Liang Zhou and**

Chaoying Zhou: contributed to study concept; **Li Ma**: contributed to study concept and design, study supervision, obtained funding, and critical revision of the manuscript. **Xinying Zhou**: contributed to study concept and design, drafting of the manuscript, study supervision, obtained funding and critical revision of the manuscript. All authors read and approved the final manuscript.

Data Availability Statement

The raw data supporting the conclusions of this article will be made available by the authors, without undue reservation.

Figure Legends

Fig. 1 Mtb activates the mitochondrial fission-related protein Drp1 to control the intracellular survival of Mtb in macrophages

(A) Confocal assay was detected the changes in mitochondrial length of mouse BMDMs labeled with MitoTracker dye after infection with H37Rv (MOI=5) for 0, 15, 30, and 60 min. Scale bar = 10 μm.

(B) Western blot was detected the expression of mitochondrial fission-related proteins at different time points after infection with Mtb at an MOI of 2.

(C) CFU assay was determined the bacterial load 48 hrs and 72 hrs after Mtb infection (MOI=5) in BMDMs with si-Fis, si-Mff, si-Mief2, si-Mief1, and si-Dnm1l knockdown respectively.

(D) Samples were collected from 6 patients with lymphatic tuberculosis, pulmonary tuberculosis, and 4 control patients with chronic inflammation, and the phosphorylation level of Drp1 in lymph node and lung tissues was detected by immunohistochemistry.

Western blot results shown in (B) and (D) are representative of n=3 biologically independent experiments using BMDMs isolated from different mice. Data are presented as mean ± SD from three independent experiments. Statistical significance was determined by one-way ANOVA followed by Tukey's post hoc test. *p ≤ 0.05, **p ≤ 0.01, ***p ≤ 0.001, ****p ≤ 0.0001; ns, not significant.

Fig. 2 Drp1 functions on macrophages and restrains Mtb infection in mice

(A, C, E, G) Western blot was detected the effect of Drp1 protein expression 24 hrs after Mtb infection (MOI=2) in si-Dnm1l-silenced, shRNA-knockdown, OE-Dnm1l cell lines, and BMDMs treated with Midivi-1.

(B, D, F, H) CFU counting was analyzed bacterial survival 48 hrs after Mtb infection (MOI=5) in si-Dnm1l-silenced, shRNA-knockdown, OE-Dnm1l cell lines, and BMDMs treated with Midivi-1.

(I) 4-week-old C57BL/6 mice were injected with Midivi-1 (20 mg/kg, i.p.; n=5 mice per group) daily and the DMSO control group, and CFU counting was used to analyze the bacterial load in the spleen and lung of mice *in vivo*.

(J) Drp1 expression of lungs in $Dnm1l^{fl/fl}$ and $Dnm1l^{Lyz2\text{-}cre}$ mice (n=5 mice per group) was detected by Western blot assay.

(A, C, E, G, J) Western blot results were representative of three independent experiments with similar results. Data shown were the mean ± SD and are from at least three independent experiments with each 3-4 replicates. Data were analyzed by T-test, $*p \leq 0.05$, $**p \leq 0.01$, $***p \leq 0.001$, ns., not significant.

(K, L, M, N, O) 4-week-old $Dnm1l^{fl/fl}$ and $Dnm1l^{Lyz2\text{-}cre}$ mice were infected with M. tuberculosis, and assessing CFU counting in the lungs, spleen weight, pulmonary inflammatory area, levels of key cytokines in lung homogenates, and the extent of infiltrating monocytes and macrophages in the lung tissue.

(K) CFU counting was used to determine the bacterial load in lung of mice at 0, 1, and 4 weeks post-infection (n=5 mice per group).

(L) Splenomegaly assessment at 4 weeks. Representative photographs of spleens (left) and quantitative spleen weight (right; n=5 mice per group).

(M, N, O) To comprehensively assess pulmonary pathology at 4 weeks post-infection, we performed a multi-faceted analysis. (**M)** Representative photomicrographs of H&E-stained lung sections are shown, with the inflammatory area quantified as a percentage of the total lung area (n=5 mice per group). (**N)** Concurrently, the levels of key cytokines (IL-1β, IL-6, TNF-α, and IL-10) in lung homogenates were measured by ELISA (n=5 mice per group). (**O)** The infiltration of myeloid cells into the lungs was quantified by flow cytometry, specifically identifying monocytes ($CD11b^{+}Ly6G^{-}Ly6C^{+}$) and macrophages ($CD11b^{+}Ly6G^{-}Ly6C^{-}$) (n=5 mice per group). Data are presented as mean ± SD from three independent experiments. Statistical significance was determined by one-way ANOVA followed by Tukey's post hoc test. *p $\leqslant$ 0.05, **p $\leqslant$ 0.01, ***p $\leqslant$ 0.001, ****p $\leqslant$ 0.0001; ns, not significant.

Fig. 3 Drp1 inhibits Mtb survival by promoting xenophagy of macrophages

(A, C, E) Western blot was detectd the effect of Drp1 on the expression of Atg7, Atg5, Becline-1, P62, and LC3 proteins 24 hrs after Mtb infection (MOI=2) in si-Dnm1l-silenced, shRNA-knockdown, and OE-Dnm1l cell lines.

(B, D, F) After si-Dnm1l-silenced, shRNA-knockdown, and OE-Dnm1l cell lines were infected with Texas red-stained Mtb at MOI=2 for 24 hrs. Nuclei were stained with DAPI (blue). Colocalization (yellow) indicates LC3-positive autophagosomes

surrounding Mtb. Representative images from n=3 biologically independent experiments (BMDMs isolated from different mice per condition) are shown. Scale bar = 10 μm. Quantification of colocalization (Pearson's correlation coefficient) was calculated from at least 20 cells per condition per experiment.

(G) Double-staining immunofluorescence assays of LC3 in $F4/80^{+}$ macrophages in the lung tissues of $Dnm1l^{fl/fl}$ and $Dnm1l^{Lyz2\text{-}cre}$ mice at 4 weeks post-infection (n=5 mice per genotype. Representative images from 5 randomly selected fields of view per mouse are shown). “Pearson’s R value” refers to Pearson’s correlation coefficient.

(H) Western blot was detected changes in LC3 protein expression in OE-Dnm1l cells pre-treated with 3-MA for 2 hrs and infected with Mycobacterium tuberculosis at MOI=2 for 24 hrs.

(I) CFU counting was analyzed bacterial survival in BMDMs transfected with OE-Drp1 and NC after pre-treatment with 3-MA for 2 hrs and infection with Mtb at MOI=5 for 48 hrs.

(A, C, E, H) Western blot results were representative of three independent experiments with similar results. Data are presented as mean ± SD from three independent experiments. Statistical significance was determined by one-way ANOVA followed by Tukey's post hoc test. *p $\leqslant$ 0.05, **p $\leqslant$ 0.01, ***p $\leqslant$ 0.001, ****p $\leqslant$ 0.0001; ns, not significant.

Fig. 4 Drp1 upregulates HIF-1α expression to promote xenophagy of macrophages

(A, B, C) Western Blot was detected the effect of Drp1 on HIF-1αprotein expression in si-Dnm1l-silenced, shRNA-knockdown, and OE-Dnm1l cell lines infected with Mtb at an MOI of 2 for 24 hrs.

(D) Western Blot was detected changes in LC3 protein expression in BMDMSs transfected with si-Drp1 and si-NC, which were treated with Roxadustat and infected with Mycobacterium tuberculosis at an MOI of 2 for 24 hrs.

(E) BMDMSs transfected with si-Drp1 and si-NC were treated with Roxadustat for and then infected with Texas red-stained Mycobacterium tuberculosis at an MOI of 2 for 24 hrs. The changes in the level of Alexa Fluor 488-labeled LC3 protein (green) and its co-localization (yellow) with Mtb (red) were detected by immunofluorescence confocal microscopy. Nuclei were stained with DAPI (blue). Colocalization (yellow) indicates LC3-positive autophagosomes surrounding Mtb. Representative images from n=3 biologically independent experiments are shown. Scale bar: 10 μm. Quantification of colocalization (Pearson's correlation coefficient) was calculated from at least 20 cells per condition per experiment.

(F) CFU counting was analyzed the survival of bacteria in BMDMSs transfected with si-Drp1 and si-NC, which were treated with Roxadustat and then infected with Mtb at an MOI of 5 for 48 hrs. Data are presented as mean ± SD from n=3 independent biological replicates, each performed with 3–4 technical replicates.

(A-D) Western blot results were representative of three independent experiments with similar results. Data are presented as mean ± SD from three independent experiments.

Statistical significance was determined by one-way ANOVA followed by Tukey's post hoc test. *$p \leq 0.05$, **$p \leq 0.01$; ns, not significant.

Fig. 5 ROS production is required for xenophagy mediated by Drp1-HIF-1α axis

(A, D, G) Western Blot was detected the effect of Drp1 on iNOS protein expression in si-Dnm1l-silenced, shRNA-knockdown, and OE-Dnm1l cells infected with Mtb at an MOI of 2 for 24 hrs.

(B, E, H) NO detection kits were detected the effect of Drp1 on NO production in si-Dnm1l-silenced, shRNA-knockdown, and OE-Dnm1l cells infected with Mtb at an MOI of 2 for 24 hrs.

(C, F, I) The level of ROS production was measured using a fluorescence microplate reader in si-Dnm1-silenced, shRNA-knockdown, and OE-Dnm1 cells infected with Mtb at an MOI of 2 for 6 hrs.

(J, N) Fluorescence microplate reader was detected the effect of Drp1 on ROS roduction in OE-Dnm1l cells infected with Mtb at an MOI of 2 for 6 hrs after treatment with L-NAME or NAC.

(K, M) NO detection kits was detected changes in NO production in OE-Dnm1l cells treated with L-NAME or NAC, which infected with Mtb at an MOI of 2 for 24 hrs.

(L, O) CFU counting was analyzed the survival of bacteria in OE-Dnm1l cells treated with L-NAME or NAC, which infected with Mtb at an MOI of 5 for 48 hrs.

(P) Western Blot was detected the expressions of HIF-1α, iNOS, and LC3 proteins in

OE-Dnm1 cells treated with NAC and infected with Mtb at an MOI of 2 for 24 hrs.

(**A, D, G, P)** Western blot results were representative of three independent experiments with similar results. Data are presented as mean ± SD from three independent experiments. Statistical significance was determined by one-way ANOVA followed by Tukey's post hoc test.*$p \leq 0.05$, **$p \leq 0.01$, ***$p \leq 0.001$, ns, not significant.

Fig. 6 Drp1 promotes autophagy flux to suppress Mtb infection

(A) Western blot analysis of LC3-II and p62 protein levels in Drp1-overexpressing macrophages treated with or without chloroquine (CQ, 30 μM, pretreatment 4 hrs). β-actin served as a loading control.

(B) Quantification of intracellular Mtb survival (CFU) in Drp1-overexpressing macrophages treated with or without CQ (CQ, 30 μM, pretreatment 4 hrs). Data are presented as mean ± SD from three independent experiments.

(C) Western Blot was detected changes in LC3 protein expression in BMDMSs transfected with si-Drp1 and si-NC, which were treated with CCCP (autophagy agonist) and then infected with Mtb at an MOI of 2 for 24 hrs.

(D) BMDMSs transfected with si-Drp1 and si-NC were treated with CCCP and then infected with Texas red-stained Mtb at an MOI of 2 for 24 hrs. Colocalization (yellow) indicates LC3-positive autophagosomes surrounding Mtb. Representative images from n=3 biologically independent experiments are shown. Scale bar = 10 μm. Quantification of colocalization (Pearson's correlation coefficient) was calculated from at least 20 cells

per condition per experiment.

(E) The mCherry-eGFP-LC3 dual-fluorescence reporter autophagic flux system was transfected with si-Drp1 and si-NC, treated with CCCP, and then infected with Mtb at an MOI of 2. Changes in autophagic flux were observed using a laser confocal microscope.

(F) Flow cytometry was detected the effect of Drp1 on ROS production in si-Drp1 and si-NC BMDMs infected with Mtb at an MOI of 5 for 6 hrs after treatment with CCCP.

(G) CFU counting was analyzed the survival of bacteria in BMDMSs transfected with si-Drp1 and si-NC, which were treated with CCCP and then infected with Mtb at an MOI of 5 for 48 hrs.

(A, C) Western blot results were representative of three independent experiments with similar results. Data are presented as mean ± SD from three independent experiments. Statistical significance was determined by one-way ANOVA followed by Tukey's post hoc test. *p $\leqslant$ 0.05, **p $\leqslant$ 0.01, ***p $\leqslant$ 0.001, ****p $\leqslant$ 0.0001; ns, not significant.

Fig. 7. Drp1 phosphorylation at Ser616 is required for ROS-dependent autophagic flux and xenophagic clearance of Mtb.

(A) Samples were collected from 6 patients with lymphatic tuberculosis, pulmonary tuberculosis, and 4 control patients with chronic inflammation, and the phosphorylation level of Drp1 in lymph node and lung tissues was detected by immunohistochemistry.

Differences between groups were analyzed using an unpaired, two-tailed Student's t-test (for two groups). *p $\leqslant$ 0.05.

(B) RAW264.7 macrophages stably expressing vector control, Drp1-Wt, or Drp1-S616A mutant were analyzed for p-Drp1 (S616), total Drp1 expression, HIF-1α, LC3-II, and p62 expression were analyzed by Western blot in cells described in by Western blot.

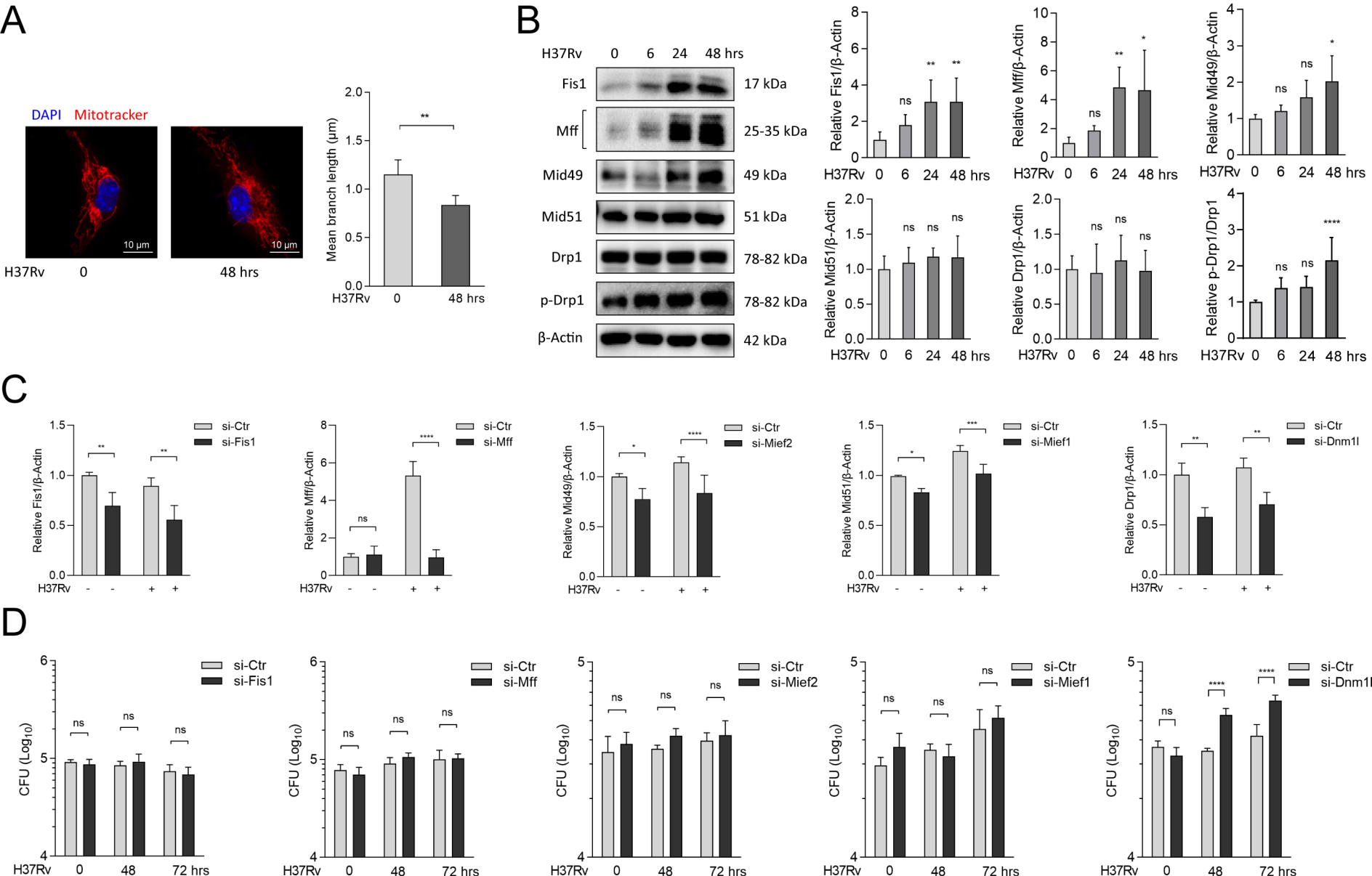
(C, D) Representative confocal images and quantification of colocalization (yellow) between Mtb (red) and Lamp1 (green) or p62 (green) in cells described in (B). Nuclei were stained with DAPI (blue). Scale bars, 10 μm.

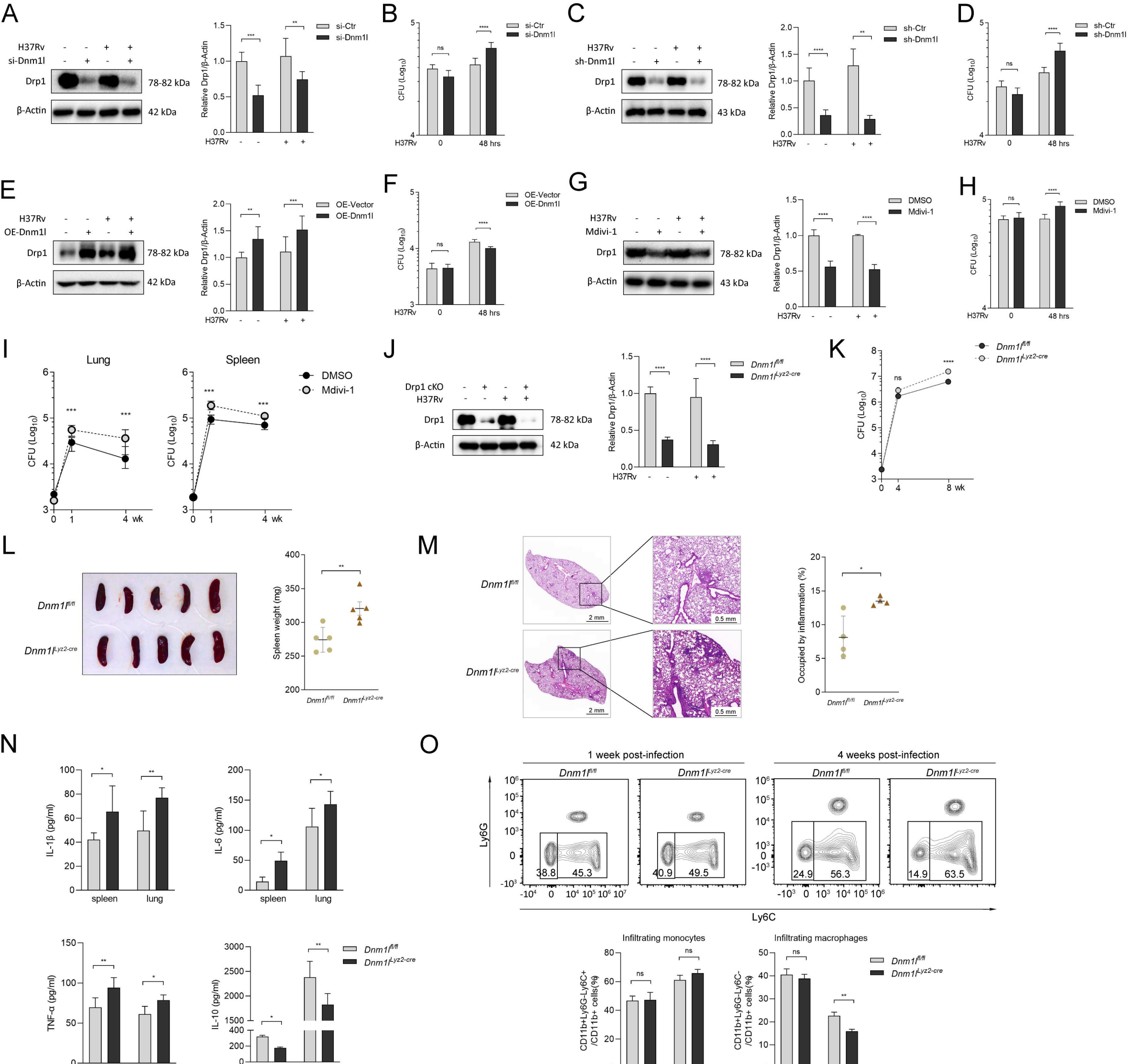
(E) ROS production was measured by DCFH-DA fluorescence in cells described in (B).

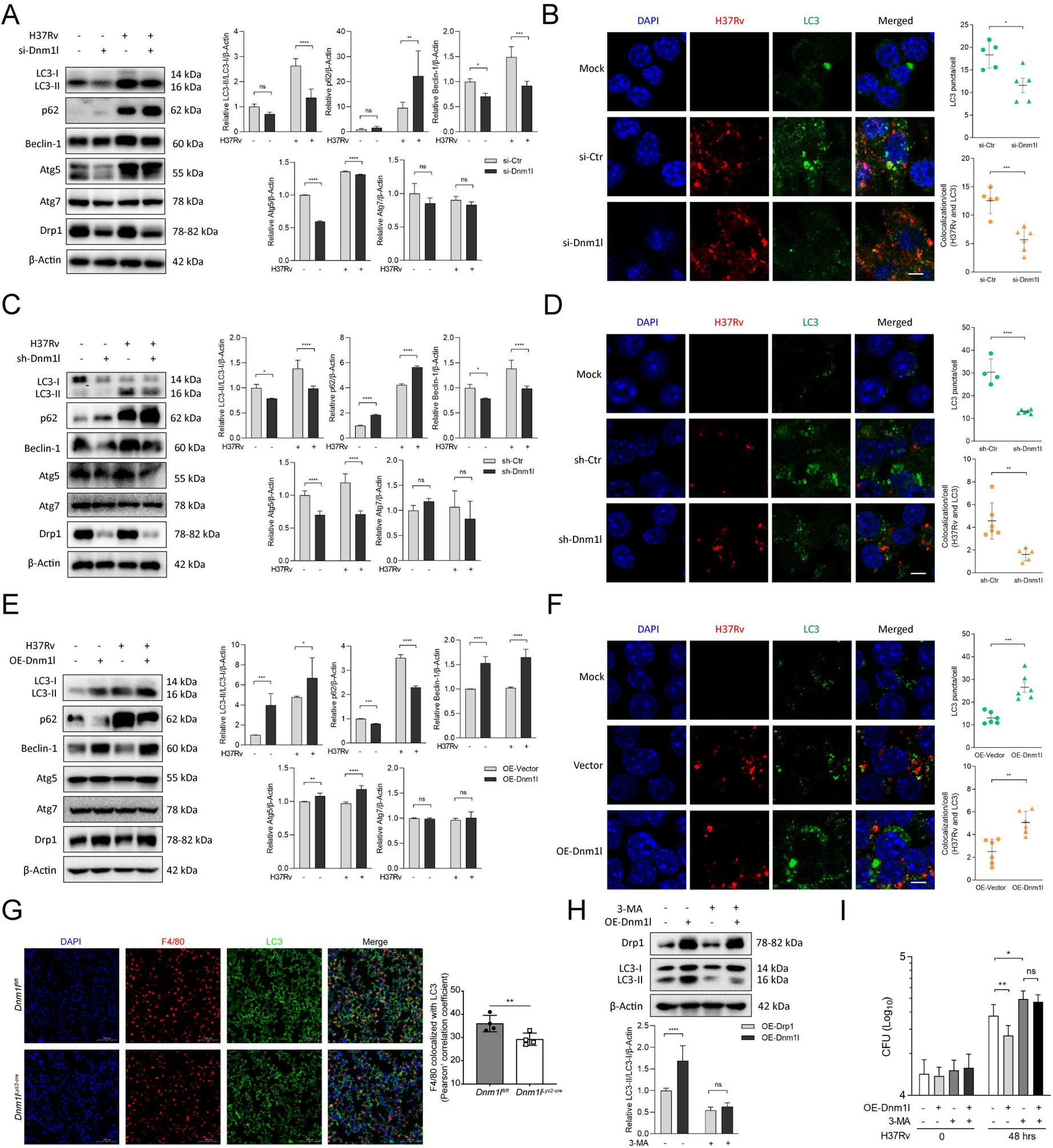
(F) Intracellular Mtb survival was determined by CFU assay in cells described in (B) at 48 hrs post-infection.

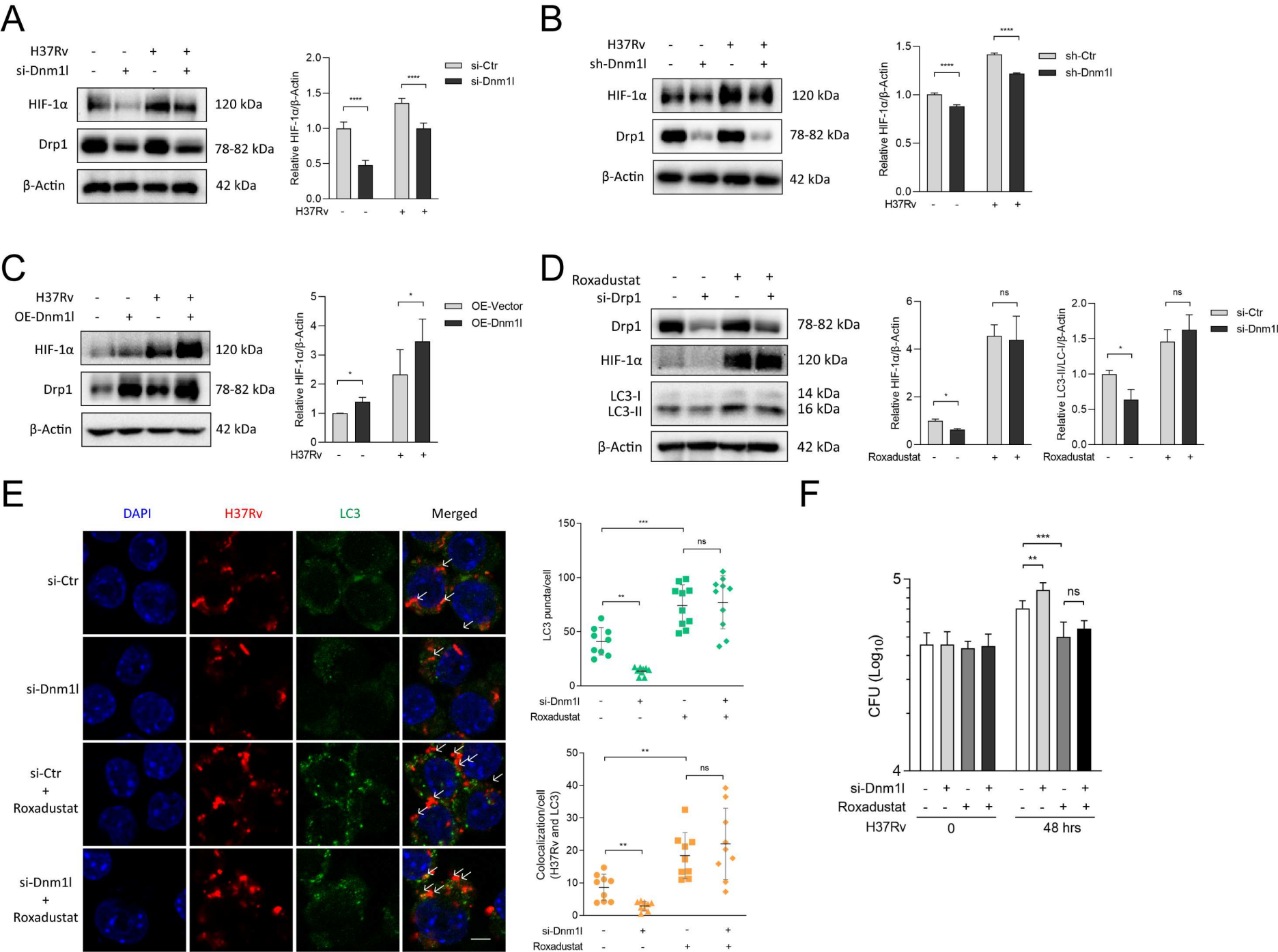
Data are presented as mean ± SD from three independent experiments. Statistical significance was determined by one-way ANOVA followed by Tukey's post hoc test. *p $\leqslant$ 0.05, **p $\leqslant$ 0.01, ***p $\leqslant$ 0.001, ****p $\leqslant$ 0.0001; ns, not significant.

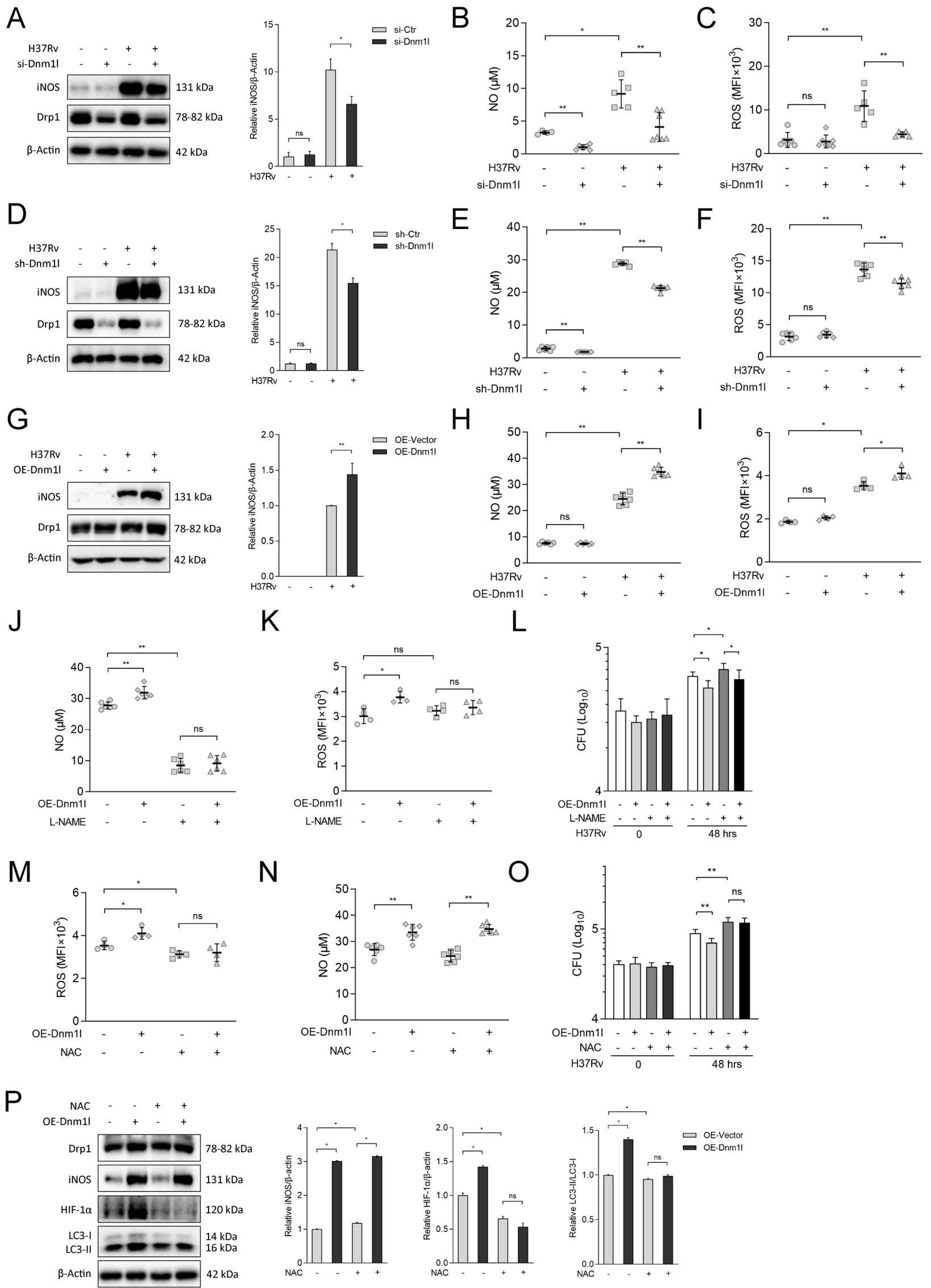
Fig. 8. Schematic model of Drp1-mediated host defense against Mtb in macrophages. Mtb infection promotes Drp1 phosphorylation at Ser616, which drives ROS production and HIF-1α stabilization. HIF-1α in turn promotes autophagic flux, leading to xenophagic clearance of intracellular Mtb. The S616A mutation abrogates this pathway, resulting in impaired bacterial clearance.

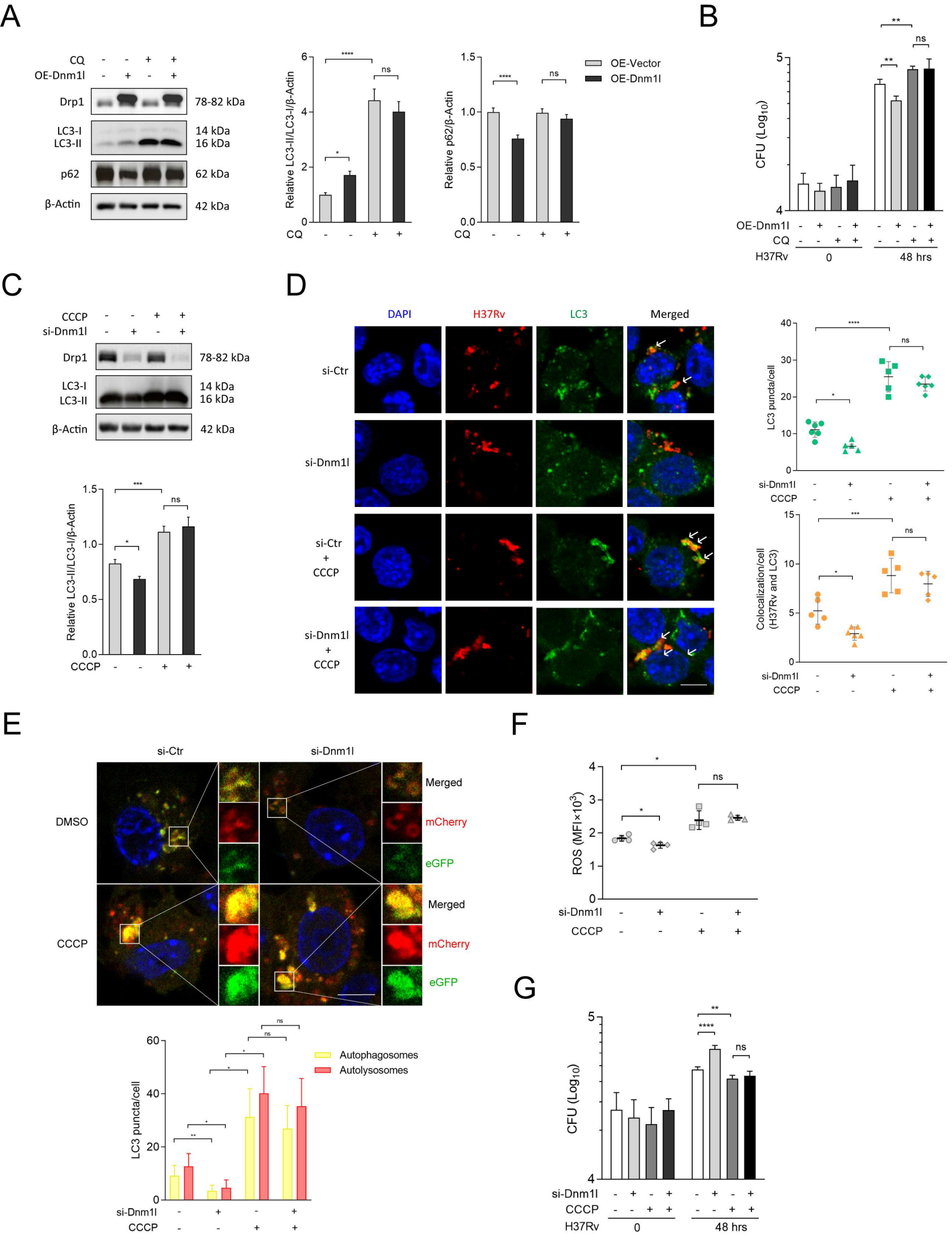

A
DAPI Mitotracker
10 μm
10 μm
H37Rv 0 48 hrs
Mean branch length (μm)
H37Rv 0 48 hrs
B
H37Rv 0 6 24 48 hrs
Fis1 17 kDa
Mff 25-35 kDa
Mid49 49 kDa
Mid51 51 kDa
Drp1 78-82 kDa
p-Drp1 78-82 kDa
β-Actin 42 kDa
Relative Fis1/β-Actin
Relative Mff/β-Actin
Relative Mid49/β-Actin
Relative Mid51/β-Actin
Relative Drp1/β-Actin
Relative p-Drp1/Drp1
C
si-Ctr
si-Fis1
si-Mff
si-Mief2
si-Mief1
si-Dnm1l
Relative Fis1/β-Actin
Relative Mff/β-Actin
Relative Mid49/β-Actin
Relative Mid51/β-Actin
Relative Drp1/β-Actin
H37Rv
D
si-Ctr
si-Fis1
si-Mff
si-Mief2
si-Mief1
si-Dnm1l
CFU (Log10)
H37Rv 0 48 72 hrs

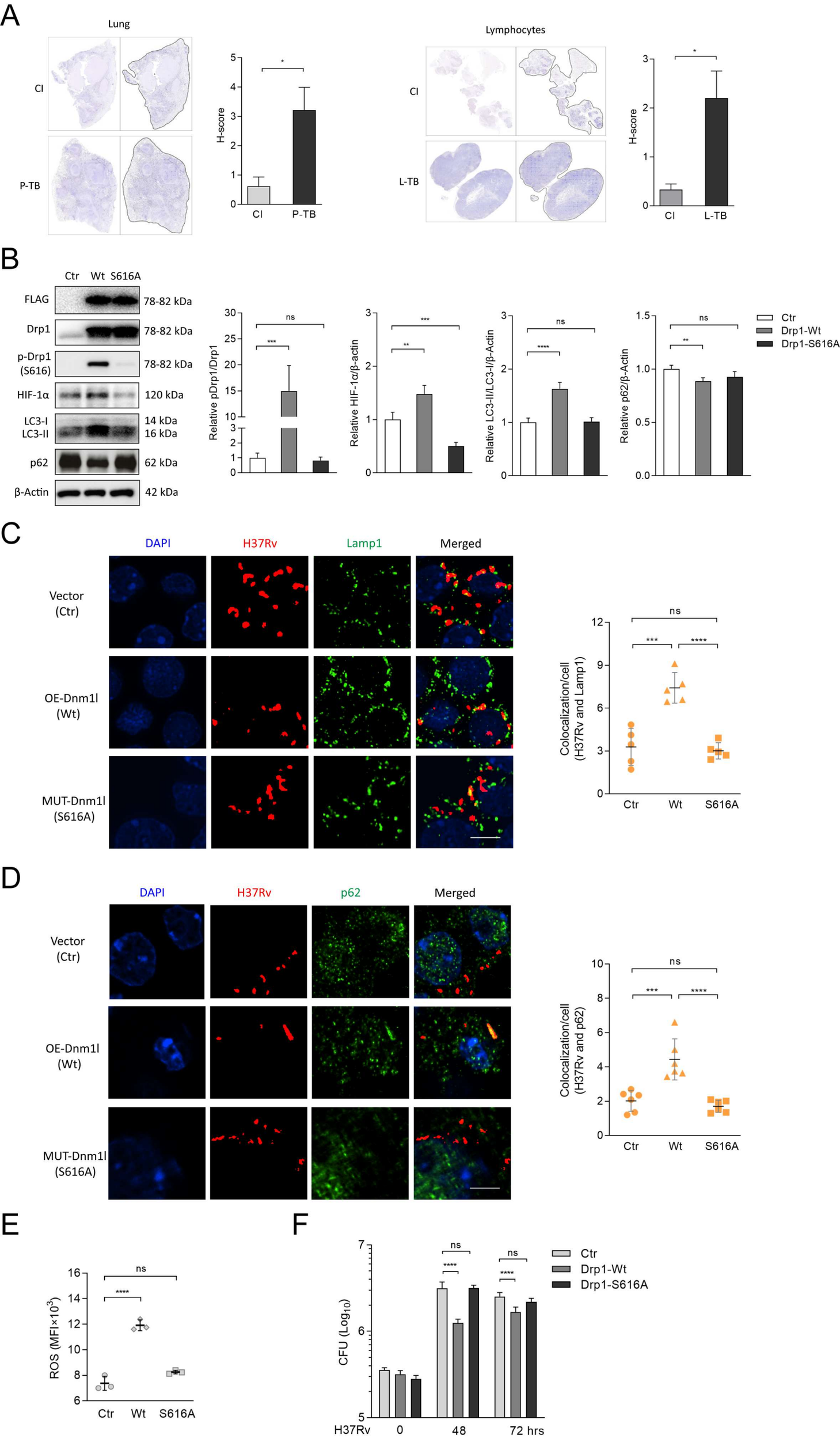

A
H37Rv
si-Dnm1l
Drp1
78-82 kDa
β-Actin
42 kDa
Relative Drp1/β-Actin
si-Ctr
si-Dnm1l
B
CFU (Log10)
ns
****
H37Rv
0
48 hrs
C
sh-Dnm1l
sh-Ctr
43 kDa
**
D
E
OE-Dnm1l
OE-Vector
OE-Dnm1l
F
G
Mdivi-1
DMSO
H
I
Lung
Spleen
DMSO
Mdivi-1
0
1
4 wk
J
Drp1 cKO
Dnm1l^fl/fl
Dnm1l^Lyz2-cre
K
8 wk
L
Spleen weight (mg)
M
2 mm
0.5 mm
Occupied by inflammation (%)
N
IL-1β (pg/ml)
IL-6 (pg/ml)
TNF-α (pg/ml)
IL-10 (pg/ml)
spleen
lung
O
1 week post-infection
4 weeks post-infection
Ly6G
Ly6C
38.8
45.3
40.9
49.5
24.9
56.3
14.9
63.5
Infiltrating monocytes
Infiltrating macrophages
CD11b+Ly6G-Ly6C+ /CD11b+ cells(%)
CD11b+Ly6G-Ly6C- /CD11b+ cells(%)

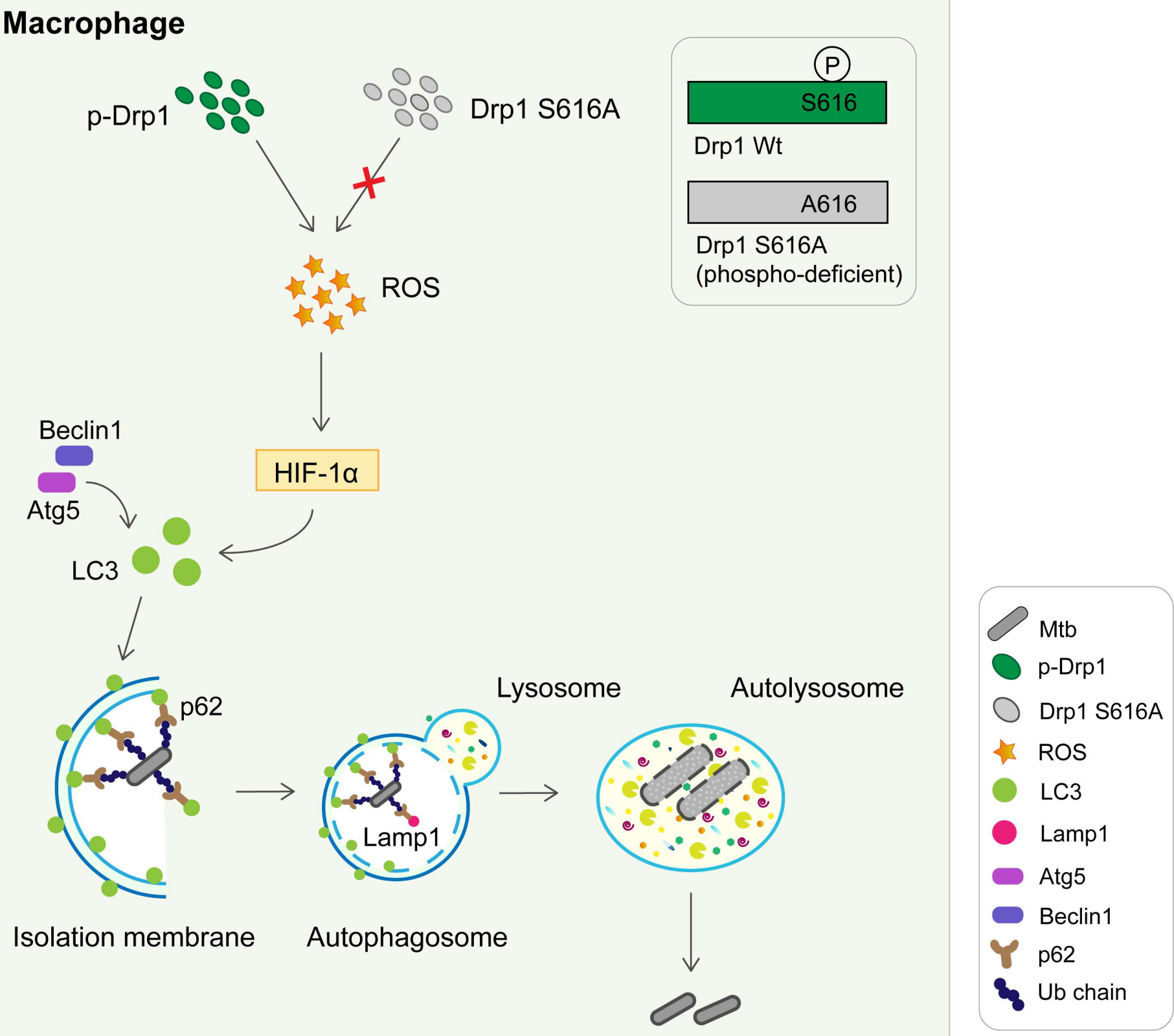

A
H37Rv
si-Dnm1l
LC3-I
LC3-II
p62
Beclin-1
Atg5
Atg7
Drp1
β-Actin
14 kDa
16 kDa
62 kDa
60 kDa
55 kDa
78 kDa
78-82 kDa
42 kDa
Relative LC3-II/LC3-I/β-Actin
Relative p62/β-Actin
Relative Beclin-1/β-Actin
Relative Atg5/β-Actin
Relative Atg7/β-Actin
si-Ctr
si-Dnm1l
B
DAPI
H37Rv
LC3
Merged
Mock
si-Ctr
si-Dnm1l
LC3 puncta/cell
Colocalization/cell (H37Rv and LC3)
C
sh-Dnm1l
sh-Ctr
sh-Dnm1l
D
E
OE-Dnm1l
OE-Vector
OE-Dnm1l
F
Vector
G
F4/80
Merge
Dnm1f/f/f
Dnm1lyz2-cre
F4/80 colocalized with LC3 (Pearson' correlation coefficient)
H
3-MA
OE-Drp1
I
CFU (Log10)
48 hrs


A
H37Rv
si-Dnm1l
HIF-1α
Drp1
β-Actin
120 kDa
78-82 kDa
42 kDa
Relative HIF-1α/β-Actin
si-Ctr
si-Dnm1l
B
sh-Dnm1l
sh-Ctr
C
OE-Dnm1l
OE-Vector
D
Roxadustat
si-Drp1
LC3-I
LC3-II
14 kDa
16 kDa
Relative LC3-II/LC-I/β-Actin
E
DAPI
H37Rv
LC3
Merged
si-Ctr
si-Dnm1l
si-Ctr + Roxadustat
si-Dnm1l + Roxadustat
LC3 puncta/cell
Colocalization/cell (H37Rv and LC3)
F
CFU (Log10)
48 hrs
ns


A
H37Rv
si-Dnm1l
iNOS
Drp1
β-Actin
131 kDa
78-82 kDa
42 kDa
Relative iNOS/β-Actin
si-Ctr
si-Dnm1l
ns
B
NO (μM)
C
ROS (MFI×10³)
D
sh-Ctr
sh-Dnm1l
E
F
G
OE-Vector
OE-Dnm1l
H
I
J
L-NAME
K
CFU (Log10)
48 hrs
M
NAC
N
O
P
HIF-1α
LC3-I
LC3-II
14 kDa
16 kDa
120 kDa
Relative HIF-1α/β-actin
Relative LC3-II/LC3-I


A
CQ
OE-Dnm1l
Drp1
78-82 kDa
LC3-I
LC3-II
14 kDa
16 kDa
p62
62 kDa
β-Actin
42 kDa
Relative LC3-II/LC3-I/β-Actin
Relative p62/β-Actin
OE-Vector
OE-Dnm1l
B
CFU (Log10)
H37Rv
0
48 hrs
C
CCCP
si-Dnm1l
D
DAPI
H37Rv
LC3
Merged
si-Ctr
si-Dnm1l
si-Ctr + CCCP
si-Dnm1l + CCCP
LC3 puncta/cell
Colocalization/cell (H37Rv and LC3)
E
si-Ctr
si-Dnm1l
DMSO
CCCP
Merged
mCherry
eGFP
Autophagosomes
Autolysosomes
F
ROS (MFI×10³)
G


A
Lung
CI
P-TB
H-score
CI
P-TB
Lymphocytes
CI
L-TB
H-score
CI
L-TB
B
Ctr
Wt
S616A
FLAG
Drp1
p-Drp1 (S616)
HIF-1α
LC3-I
LC3-II
p62
β-Actin
78-82 kDa
78-82 kDa
78-82 kDa
120 kDa
14 kDa
16 kDa
62 kDa
42 kDa
Relative pDrp1/Drp1
Relative HIF-1α/β-actin
Relative LC3-II/LC3-I/β-Actin
Relative p62/β-Actin
Ctr
Drp1-Wt
Drp1-S616A
C
DAPI
H37Rv
Lamp1
Merged
Vector (Ctr)
OE-Dnm1l (Wt)
MUT-Dnm1l (S616A)
Colocalization/cell (H37Rv and Lamp1)
Ctr
Wt
S616A
D
DAPI
H37Rv
p62
Merged
Vector (Ctr)
OE-Dnm1l (Wt)
MUT-Dnm1l (S616A)
Colocalization/cell (H37Rv and p62)
Ctr
Wt
S616A
E
ROS (MFI×10³)
Ctr
Wt
S616A
F
CFU (Log10)
H37Rv
0
48
72 hrs
Ctr
Drp1-Wt
Drp1-S616A


Macrophage
p-Drp1
Drp1 S616A
P
S616
Drp1 Wt
A616
Drp1 S616A
(phospho-deficient)
ROS
Beclin1
Atg5
HIF-1α
LC3
p62
Lysosome
Autolysosome
Lamp1
Isolation membrane
Autophagosome
Mtb
p-Drp1
Drp1 S616A
ROS
LC3
Lamp1
Atg5
Beclin1
p62
Ub chain

Supplementary Files

This is a list of supplementary files associated with this preprint. Click to download.

- SupplementaryMaterial.docx